Chemical Engineering Journal 392 (2020): 124867

DOI: https://doi.org/10.1016/j.cej.2020.124867

Degradation pathways of emerging contaminants using TiO_2-activated carbon heterostructures in aqueous solution under simulated solar light

M. Peñas-Garzón, A. Gómez-Avilés, C. Belver*, J.J. Rodriguez, J. Bedia

Chemical Engineering Department, Universidad Autónoma de Madrid, Campus Cantoblanco, E-28049 Madrid, Spain

*Corresponding author. E-mail address: carolina.belver@uam.es

Keywords: Activated carbon; TiO_2/carbon-heterostructures; solar photocatalysis; water treatment; pharmaceutical degradation pathways.

Abstract

This work deals with the degradation of three emerging contaminants (acetaminophen, ibuprofen and antipyrine) in water under simulated solar light using different catalysts of TiO_2/activated carbon heterostructures. The heterostructures, based on anatase phase, were successfully synthesized following three different methods (solvothermal, microwave-assisted and sol-gel), using lignin as carbon precursor. The sol-gel photocatalyst only yielded 50% conversion of acetaminophen and a low mineralization (15%), probably due to the higher crystal and particle sizes and lower surface area of this heterostructure, as a consequence of the higher temperature reached during the heat-treatment included in this synthesis route to achieve anatase crystallization. In contrast, the heterostructure prepared by the microwave-assisted procedure achieved complete conversion after 6 h of reaction. Regarding the contaminants, ibuprofen was the most easily removed, requiring 3 h for complete disappearance, while antipyrine showed the highest resistance to photodegradation, not being completely removed after 6 h. The photocatalytic performance was also evaluated for a mixture of these three pharmaceuticals at different initial pH. The fastest and highest mineralization (ca. 50 %) occurred around neutral pH. The study proposes the oxidation degradation pathways of the three pharmaceuticals under solar-simulated irradiation from the analysis of the reaction intermediates.

1. Introduction

The awareness about the presence of contaminants of emerging concern (CECs) in water bodies is strongly increasing, especially in the last two decades. This type of compounds, also known as emerging contaminants due to recent detection and quantification in water streams, are considered to be biologically active, altering the metabolism of living beings, despite they are usually detected in very low concentrations [1–5]. CECs include, among other species, pharmaceuticals and personal care products that are considered endocrine disruptors and can cause negative effects on health and aquatic environments due to their continuous release [6,7]. They are commonly present in sewage and wastewater treatment plants (WWTPs) allow only partial removal in most cases, so that continuous municipal discharges give rise to accumulation in the receiving water bodies. The average removal of antibiotics in WWTPs has been reported in the range of 40-60% and close to 25-55% in the case of analgesics and anti-inflammatories [8,9]. These species can be also present in the wastewaters from pharmaceutical plants, in this case at substantially higher concentrations, in the order of $mg \cdot L^{-1}$. The growing concern about water quality promotes action plans by United Nations [10] and research efforts on the development of efficient and sustainable technologies for the abatement of those pollutants, in general of hazardous character.

Several advanced treatments have been investigated for the removal of CECs [11,12], including advanced oxidation processes (AOPs), which degrade contaminants via generation of reactive oxygen species (ROS). Among the AOPs, heterogeneous photocatalysis has been widely reported for the removal of many different types of contaminants [13]. In this technology, ROS can be generated upon light absorption in a semiconductor (being TiO_2 the most used so far) giving rise to separation of electron-hole charges. Nowadays, there is a growing trend to use solar light as renewable and sustainable energy source, reducing the operation costs [8]. In spite of the wide use of TiO_2 (due to its well-stated physical and chemical properties), this material has the main drawbacks of low adsorption capacity, limited photocatalytic activity under visible light and difficult recovery from the aqueous medium, especially in the case of commercial TiO_2 [14]. Supporting TiO_2 on porous materials, as activated carbons (ACs), zeolites or clays, can partly overcome these drawbacks [15,16]. ACs are characterized by their relatively low cost, high surface area and well-developed porosity. Moreover, activated carbons can be prepared from almost any carbonaceous waste, providing a way of

valorization of those residues. Lignin, a biopolymer with relatively high carbon content is a main component of lignocellulosic biomass. Different types of modified lignin are produced in huge amounts from cellulose pulp manufacture, being mostly used by its fuel value. The future development of biorefinery is expected to generate high quantities of waste lignin whose valorization becomes mandatory. Regarding valorization possibilities, lignin has been studied as precursor for the synthesis of activated carbons and other carbon-based materials [17–26]. In a recent work [27], our research group investigated the use of different activating agents ($FeCl_3$, $ZnCl_2$, H_3PO_4 and KOH) in the preparation of activated carbons from lignin for synthesizing TiO_2/activated carbon heterostructures. It was observed that the photocatalyst obtained with $FeCl_3$-activated carbon yielded higher removal of acetaminophen (around 29, 42 and 74% higher than those obtained with KOH-, H_3PO_4- and $ZnCl_2$-derived carbons, respectively, after 3 h under solar light). In that previous research, the photocatalytic performance of bare TiO_2 was already studied, being higher than the synthesized TiO_2/AC heterostructures, which was attributed to a better contact of contaminant with non-supported TiO_2 as corroborated in literature [28]. However, the photocatalyst obtained with $FeCl_3$-activated carbon showed around 5-fold increment in the initial settling velocity compared to bare TiO_2, and therefore it is much easily recovered from the reaction media.

The preparation of the TiO_2/AC heterostructures can be addressed by different methods [29–32]. The properties of these heterostructures depend on the synthesis route because of the different conditions used. For instance, sol-gel synthesis requires high temperature post-treatment to obtain the highly-photoactive anatase phase; solvothermal synthesis uses lower temperatures, while microwave-assisted methodology allows a faster heating rate and different distribution of heat involving hot spots [28]. To the best of our knowledge, a detailed comparative study of the performance of TiO_2-carbonaceous heterostructures prepared by these three synthesis routes on the photocatalytic degradation of emerging contaminants has not been reported before. Additionally, in many cases it has not been established a clear difference between the contribution of adsorption and photodegradation, despite this can be a key factor when using highly porous materials as catalyst supports. In the current study, TiO_2/AC heterostructures have been synthesized by three different methods (solvothermal, microwave-assisted and sol-gel), being the activated carbon previously prepared by chemical activation of lignin with $FeCl_3$. The synthesized heterostructures have been tested in the solar-driven photocatalytic

degradation of three target pharmaceuticals (acetaminophen, ibuprofen and antipyrine), paying special attention to the effect of pH and the extent of mineralization. Experiments with three single compounds as well as with mixtures of them have been performed. In addition to this, intermediates of the photocatalytic oxidation of individual contaminants were identified, being proposed the degradation pathways of these pharmaceuticals under solar-simulated light.

2. Materials and Methods

2.1. Materials

The activated carbon used was synthesized from lignin (supplied by LignoTech Iberica S.A.) as carbon source and $FeCl_3 \cdot 6H_2O$ (≥97%, Panreac) as activating agent. Ethanol (EtOH; 96%, Panreac) was used as solvent in the synthesis of the heterostructures. Titanium tetrabutoxide ($Ti(OBu)_4$; ≥97%) and titanium isopropoxide ($Ti(OiPr)_4$; ≥97%) were used as titania precursors and both were supplied by Sigma Aldrich. The photocatalytic performance was tested in the degradation of acetaminophen (ACE; ≥99%), ibuprofen (IBU; ≥98%) and antipyrine (ANT; ≥99%), all purchased from Sigma Aldrich (their chemical structures can be seen in Figure S1 of the Supplementary Information). NaOH (≥95%) and HCl (≥37%) were used as pH-modifiers and purchased from Scharlau and Sigma Aldrich, respectively. NaCl (>99.5%) was supplied by Panreac. The mobile phase for liquid chromatography consisted of acetic acid (≥99%, Sigma Aldrich) and acetonitrile (ACN, HPLC grade, Scharlau). Finally, ultrapure water (Type I, 18.2 MΩ·cm) and deionized water (Type II) were used throughout the work.

2.2. Preparation of activated carbon (AC)

Following our previous results on the synthesis of TiO_2/AC heterostructures [27], we selected $FeCl_3$ as activating agent to prepare the lignin-derived AC [33–35]. Lignin and $FeCl_3$ (1:3 mass ratio) were physically mixed and dried at 60 ºC overnight. Then, the mixture was heat-treated using a horizontal stainless-steel tubular furnace at 800 ºC (heating rate of 10 ºC·min^{-1}) for 2 h under inert atmosphere (N_2, 150 cm^3 STP·min^{-1}). After cooling, the resulting material was firstly washed with 0.1 M HCl at 70 ºC for 2 h to remove the residual activating agent and free the porosity. Then, it was rinsed to neutral pH using ultrapure water at room temperature. The activated carbon was finally dried at 60 ºC overnight, stored and labelled as AC.

2.3. Synthesis of TiO_2/AC heterostructures

Three different routes were followed to prepare the TiO_2/AC heterostructures. In all cases, a TiO_2:AC mass ratio of 4:1 was used [27]. Other TiO_2:AC mass ratios were also tested, but 4:1 led to the best photocatalysts. The amount of water was stoichiometrically fixed to promote the hydrolysis and condensation of the titania precursor.

2.3.1. Solvothermal (ST) route.

The solvothermal synthesis of the TiO_2/AC heterostructure has been described elsewhere [27]. Briefly, a suspension (A1) of 58 mg of AC in 45 mL of EtOH was firstly prepared at room temperature. Then, a solution (B1), obtained by diluting 1 mL of $Ti(OBu)_4$ in 15 mL of EtOH, was added to A1 under continuous stirring. Subsequently, 3 mL of ultrapure water were added to 15 mL of EtOH (solution C1) dropwise to hydrolyze the $Ti(OBu)_4$. Finally, the mixture was stirred for 5 min, placed in a 125 mL Teflon-lined stainless-steel autoclave and heated at 160 ºC for 3 h in an oven (Memmert UN30). The resulting solid was separated by centrifugation (5300 rpm, 10 min) and washed once with EtOH and four times with ultrapure water. The sample was finally dried at 60 ºC overnight and labelled as TiO_2/AC-ST.

2.3.2. Microwave-assisted (MW) route.

The microwave-assisted route was based on the method described by Orha et al. [32]. In this synthesis, 37.1 mg of AC were suspended in 28.5 mL of EtOH (solution A2). Other two solutions were prepared by diluting 0.633 mL of $Ti(OBu)_4$ in 9.5 mL of EtOH (solution B2); and 1.9 mL ultrapure water into 9.5 mL of EtOH (solution C2). Then, A2 and B2 were mixed under continuous stirring, while C2 was further dropwise incorporated. The final mixture was transferred to a 100 mL Teflon-lined reactor and then inserted in a SK-15 Microwave Digestion Rotor (Milestone). The synthesis was performed setting 175 ºC as constant temperature (600 W as maximum microwave power input) for 30 min. The resulting solid was separated by centrifugation, washed and dried as described for the previous solvothermal route. The resulting material was named as TiO_2/AC-MW.

2.3.3. Sol-gel (SG) route.

The sol-gel synthesis of TiO_2/AC heterostructure was slightly modified from a previous work of Belver et al. [16]. In this method, a suspension of 67.2 mg of AC in 12.5 mL of

EtOH was firstly prepared (solution A3); then, 1 mL of $Ti(OiPr)_4$ was added to 1.9 mL of EtOH (solution B3). Meanwhile, solution C3 was prepared adding 0.25 mL of ultrapure water to 1.75 mL of EtOH. A3 and B3 were mixed under stirring in a 100 mL glass beaker while C3 was slowly added favoring homogenous dispersion. The beaker was sealed with parafilm and the mixture was then heated at 50 ºC during 72 h, under stirring. During this time, a dense gel was obtained after the spontaneous coagulation of the mixture. Thereafter, the gel was dried at room temperature for 72 h. The resulting solid was heat-treated at 500 ºC for 2 h under inert atmosphere (N_2, 150 cm^3 STP·min^{-1}) inside a horizontal stainless-steel tubular furnace. The resulting heterostructure was labelled as TiO_2/AC-SG. In this synthesis, $Ti(OiPr)_4$ was selected as titania precursor due to the faster hydrolyzation of $Ti(OBu)_4$ in contact with water, which gives rise to the formation of high-size agglomerates of titanium oxyhydroxides. This precursor makes difficult obtaining anatase phase with low crystal size. $Ti(OiPr)_4$, whose hydrolysis rate is lower, allowing to obtain the desired anatase with low crystal size.

2.4. Characterization of the photocatalysts.

Elemental analysis was carried out in a LECO CHNS-932 to determine the content of carbon (C) in the synthesized samples. The quantification of TiO_2 in the different heterostructures was accomplished by wavelength-dispersive X-ray fluorescence (WDXRF) using a Bruker S8 TIGER spectrometer under inert atmosphere (He) with a maximum voltage of 60 kV and a maximum current of 170 mA. Spectra Plus (v. 3) software was used to determine the composition of the materials. A Bruker D8 diffractometer was used to obtain the X-ray diffraction (XRD) patterns, using Cu-Kα (λ = 0.154 nm) source (2θ range from 5 to 70º, scan step of 5º·min^{-1}). The most intense diffraction peak (101) of anatase phase was used to estimate the average crystal size (D) using the Scherrer's equation. The morphology of the heterostructures was observed by scanning electron microscopy (SEM) using a Quanta 3D Field Emission Gun (FEG) microscope (FEI Company). The distribution of TiO_2 particle size was obtained from SEM micrographs using ImageJ software, taking several images to obtain a representative result. A Micromeritics TriStar 123 static volumetric system was used to obtain the N_2 adsorption-desorption isotherms at −196 ºC after outgassing the samples under vacuum at 150 ºC overnight in a Florprep 060 Micromeritics equipment. The Brunauer-Emmett-Teller (BET) method [36] was used to obtain the specific surface area (S_{BET}), whereas both microporous (S_{MP}) and non-microporous surface area (S_{EXT}) were calculated by the t-

plot method [37]. Total pore volume (V_T) was estimated by the amount of nitrogen adsorbed at a relative pressure (P/P_0) of 0.99. UV-vis diffuse reflectance spectra (UV-vis DRS) were recorded in a Shimadzu 2501PC UV–vis spectrophotometer in the 250–800 nm wavelength range using $BaSO_4$ as reference material. The band gap (E_g) values of the heterostructures were obtained from the UV-vis DRS spectra, through the Tauc Plot method [38], considering the synthesized photocatalysts as indirect semiconductors [39]. The pH at the point of zero charge (pH_{pzc}) was determined by the pH drift method [27,40]. The photoluminescence (PL) spectra of the powder samples were obtained in a Perkin Elmer LS50B spectrofluorometer using an excitation wavelength of 275 nm and a sample holder with a quartz window.

2.5. Photocatalytic performance

The photocatalytic activity of the different heterostructures was evaluated for the degradation of acetaminophen (ACE), ibuprofen (IBU) and antipyrine (ANT) under solar-simulated irradiation. A 500 mL Pyrex closed jacketed reactor was placed inside a Suntest XLS+ (Atlas), under continuous stirring and controlled temperature (25 ºC) with a refrigerated/heating circulator 200F (Julabo). The irradiation intensity, provided by a Xe lamp (765–250 $W \cdot m^{-2}$) with a "Daylight" filter (restrains $\lambda \leq 290$ nm), was fixed at 600 $W \cdot m^{-2}$ (107.14 klx). In a typical experiment, the concentration of the photocatalyst was adjusted to 250 $mg \cdot L^{-1}$ of TiO_2, considering to the composition of the heterostructures as obtained by WDXRF. Thereafter, the photocatalyst was dispersed in a deionized water solution (150 mL) of the selected contaminant at natural pH, being 6.78, 7.05 and 7.08 for ACE, IBU and ANT, respectively. Prior to these experiments, it was observed that each heterostructure showed different adsorption capacity. Consequently, each photocatalyst was dispersed in solutions with different initial concentrations of each contaminant, in order to adjust the concentration of each contaminant at 5 $mg \cdot L^{-1}$ before starting the irradiation (after adsorption equilibrium). Finally, the photocatalytic experiments were carried out for 6 h under simulated solar light. The experiments were all performed by triplicate and the 95% confidence interval was included. Specific experiments were carried out with a mixture of the three pharmaceuticals, setting the initial concentration of each compound to 5 $mg \cdot L^{-1}$ and adjusting the pH values from 3 to 11 with diluted HCl or NaOH.

At different irradiation times, samples of 450 µL were extracted from the reaction medium and filtered using Whatman 0.2 µm PTFE syringeless filters (Scharlau). A Shimadzu Prominence-I LC-2030C (diode array detector (SPD-M30A)), was used to analyze the aliquots of the reaction by High Performance Liquid Chromatography (HPLC), using a reverse phase C18 column. A mixture of acetonitrile/acetic acid 0.1% v/v was used as mobile phase (0.7 $mL \cdot min^{-1}$). A gradient method 10/90–40/60% was used for the quantification of ACE and ANT (detection λ = 246 and 242 nm, respectively), while IBU was determined by an isocratic 50/50% method (λ = 270 nm). On the other hand, a Shimadzu TOC-L analyzer was used to measure the total organic carbon (TOC) at the beginning (TOC_0) and end (TOC_f) of each photocatalytic test. Thus, the mineralization of the contaminants was followed by the TOC removal (%). The intermediate products from the pharmaceuticals tested were identified by Liquid Chromatography followed by Electrospray Ionization-Mass spectrometry (LC/ESI-MS). A Bruker Maxis II system with electrospray ionization (ESI) was used in positive ionization mode to follow the intermediates of ACE and ANT, whereas negative ionization mode was used for IBU (due to the presence of the carboxylic acid group). The analyses were performed with a capillary voltage of 3,500 V and an end plate offset of 500 V, at 300 ºC and 8 $mL \cdot min^{-1}$ of dry gas flow. Experimental data were collected in the range from 50 to 3,000 m/z with a full scan analysis of 0.1 s and a collision energy of 30 eV. Short-chain carboxylic acids and inorganic ions ~~they~~ were detected and quantified by ionic chromatography (IC), using a Metrohm 790 IC chromatograph with a Metrosep A Supp 5 (250 mm x 4 mm) column (Metrohm). As anionic eluent was used a 0.7 $mL \cdot min^{-1}$ aqueous solution of $Na_2CO_3/NaHCO_3$ (3.2 mM/1.0 mM) and H_2SO_4 (100.0 mM) as anionic suppressor.

3. Results and Discussion

3.1. TiO_2/AC heterostructures characterization

Table 1 summarizes the TiO_2 and C contents of the different heterostructures, whose values are quite similar to the nominally expected (TiO_2:AC mass ratio of 4:1) regardless of the synthetic route used. The three samples showed the characteristic peaks of the TiO_2 anatase phase (JCPDS 78-2486), as can be observed in the diffraction patterns depicted in Figure 1. It is important to remark that neither solvothermal (TiO_2/AC-ST) nor microwave-assisted (TiO_2/AC-MW) synthesis require of an additional high-temperature

heating step to obtain the anatase phase of titania. No other TiO_2 crystalline phases (rutile or brookite) were observed in any of the heterostructures. This result contrasts with previous studies on microwave-assisted synthesis of TiO_2 on activated carbons [41,42] that yielded titania in both anatase and rutile phases. The development of anatase as the only crystalline phase can be attributed to the fact that the synthesis route used in the current work was temperature-controlled, in contrast with those other studies where power-controlled approaches were used, implying higher temperatures and further crystallization into rutile. The average crystal size (D, Table 1) was calculated from the Scherrer's equation applied to the most intense peak of anatase (101). The crystal size of TiO_2 in the sol-gel sample (TiO_2/AC-SG) was more than two-fold the obtained for solvothermal and microwave-assisted heterostructures, which can be ascribed to the heat-treatment step at 500 ºC required to transform the titanium oxyhydroxide of the dried gel into titania. The TiO_2 crystal size in TiO_2/AC-ST and TiO_2/AC-MW (c.a. 10 nm) are similar to those previously reported for other supported titania photocatalysts from hydrothermal and microwave-assisted synthesis [30,32].

Table 1. Carbon and TiO_2 content, average crystal size (D) and band gap values (E_g) of the heterostructures.

Heterostructure	%C	%TiO_2[a]	D (nm)[b]	E_g (eV)
TiO_2/AC-ST	20.1	75.9	10.1	3.38
TiO_2/AC-MW	18.6	78.6	9.0	3.35
TiO_2/AC-SG	17.9	77.2	24.4	3.28

[a] Obtained by WDXRF. [b] From (101) anatase diffraction peak.

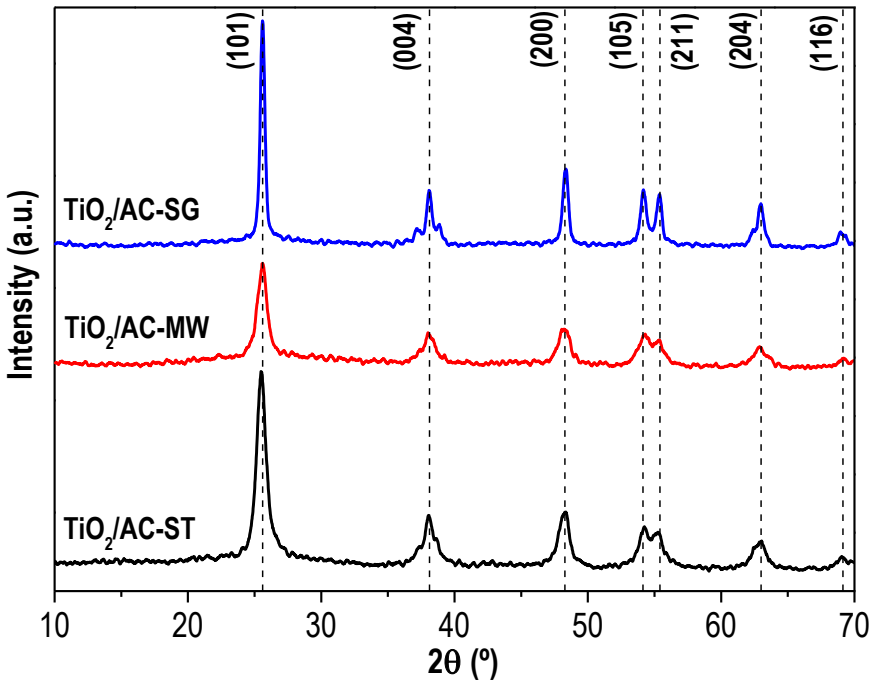

Figure 1. XRD patterns of the TiO_2/AC heterostructures. The characteristic diffraction peaks of anatase phase (JCPDS 78–2486) have been included.

Low-magnification SEM-images (Figure S2, Supplementary Information) revealed that the synthesized photocatalysts consisted of spherical TiO_2 nanoparticles distributed on the activated carbon surface. Figure 2 shows higher-magnification SEM micrographs and TiO_2 particle size distributions for the different heterostructures. The mean size of the TiO_2 particles decreased following the order: TiO_2/AC-SG (0.32 μm) > TiO_2/AC-MW (0.27 μm) > TiO_2/AC-ST (0.24 μm). Besides the highest TiO_2 particle size, TiO_2/AC-SG showed a broader distribution and much more uniform surface than the other heterostructures. These features can be ascribed to the aforementioned heat-treatment step, which removes the organic matter of the titanium precursor and caused its dehydroxylation, resulting in particle sinterization with a smoother surface. The TiO_2 mean particle size obtained in this work by microwave-assisted route is quite similar to those reported by Horikoshi et al. [43], who synthesized TiO_2 particles of ca. 0.25 μm at 180 ºC. Nevertheless, the TiO_2 particle size of TiO_2/AC-ST is higher than the reported by Liu et al. [30] for other TiO_2/commercial AC heterostructure prepared by hydrothermal synthesis.

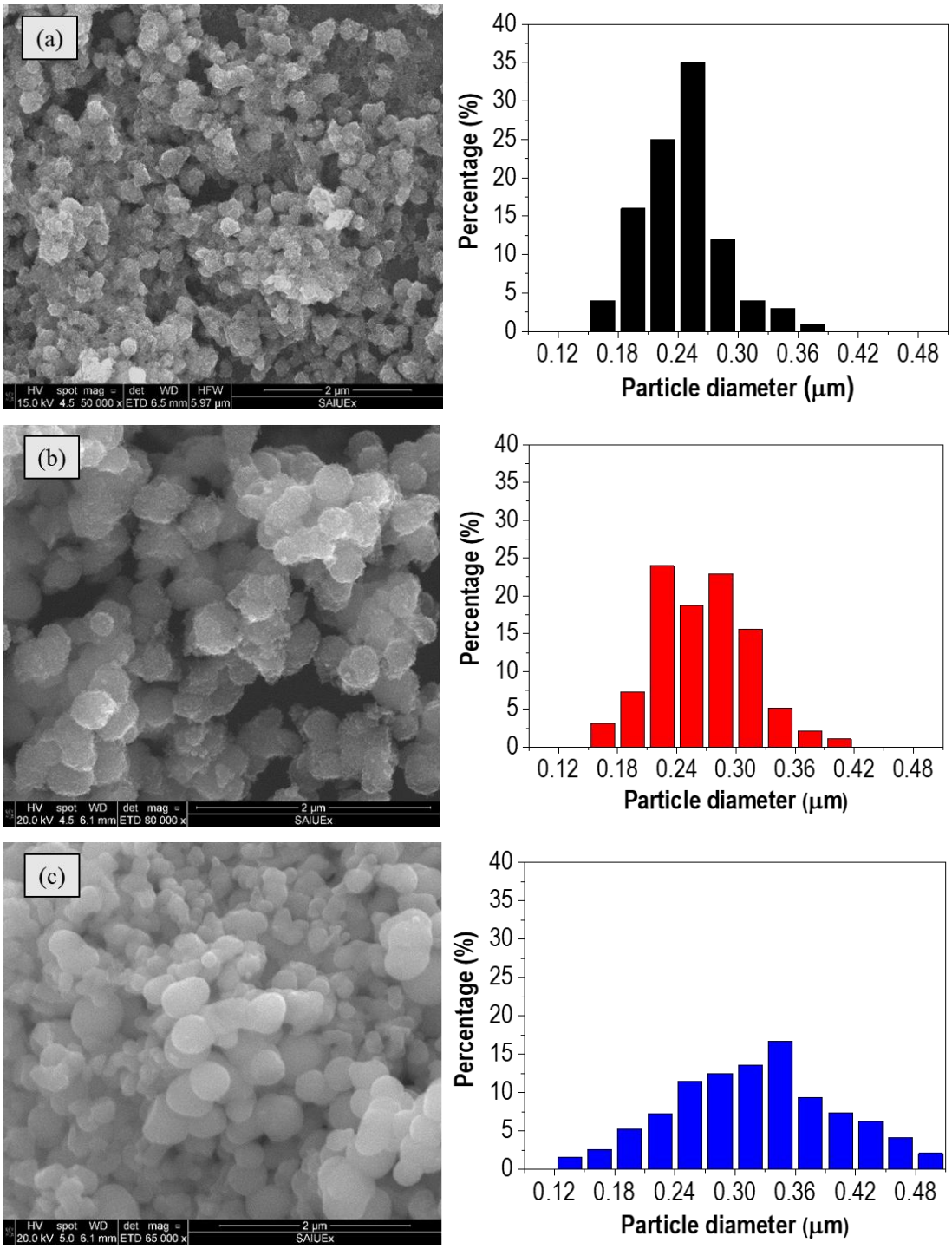

Figure 2. SEM micrographs and TiO_2 particle size distributions of the heterostructures: (a) TiO_2/AC-ST, (b) TiO_2/AC-MW and (c) TiO_2/AC-SG.

Figure 3 shows the -196 ºC N_2 adsorption-desorption isotherms of the activated carbon used as support and the three heterostructures synthesized. Meanwhile, Table 2 summarizes the porous textural characteristics derived from those isotherms. The AC showed a predominantly microporous texture with some minor contribution of

mesoporosity. This porous texture is comparable to the previously obtained from $FeCl_3$ activation of Tara gum [33] or sewage sludge [34]. On the other hand, both TiO_2/AC-ST and TiO_2/AC-MW exhibit type IV isotherms [44], characteristic of porous materials with contribution of both micro- and mesoporosity. It must be recalled that these heterostructures consist of almost 80% of TiO_2 and around 20% of AC. Thus, most of their porous texture is related to the porosity of the TiO_2 component and therefore controlled by the conditions for synthesizing the TiO_2 phase. The higher S_{EXT} values of TiO_2/AC-MW and TiO_2/AC-ST are a consequence of the higher amount of mesopores of these photocatalysts, as indicates the slope of their N_2 adsorption isotherms in the medium to high relative pressure range. Meanwhile, the TiO_2/AC-SG heterostructure showed a type I isotherm, indicative of a microporous solid. Its much lower porosity and surface area than the two other heterostructures, in spite of the quite similar TiO_2 and C contents, can be due to the heat treatment used for the crystallization of TiO_2. Martins et al. [45] reported quite similar values for a sol-gel synthesized TiO_2/activated carbon materials.

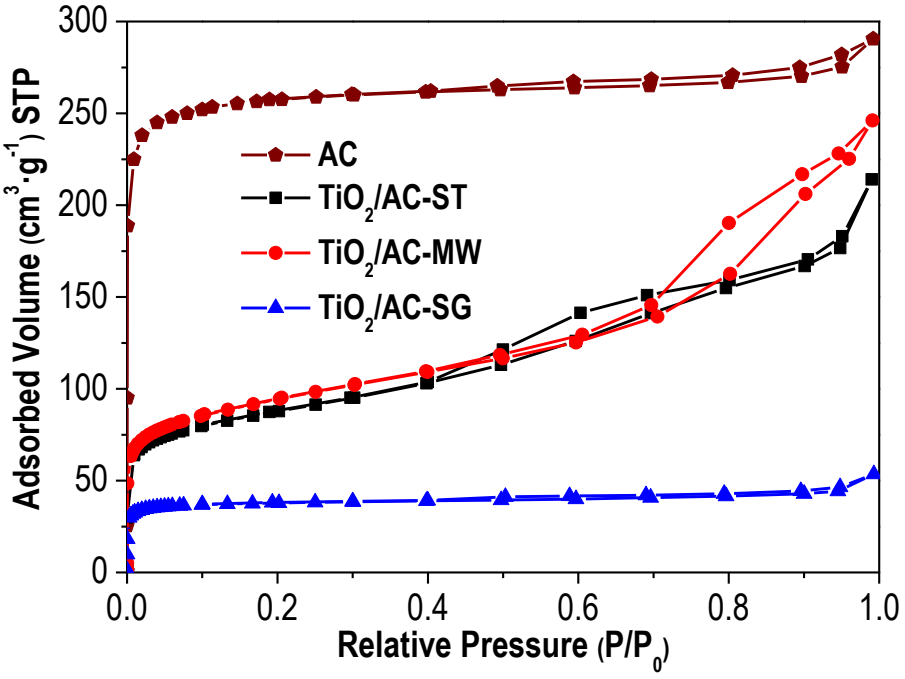

Figure 3. -196 ºC N_2 adsorption-desorption isotherms of the activated carbon (AC) and the TiO_2/AC heterostructures.

Table 2. Characterization of the porous texture of the AC and the heterostructures.

Sample	S_{BET} ($m^2 \cdot g^{-1}$)	S_{MP} ($m^2 \cdot g^{-1}$)	S_{EXT} ($m^2 \cdot g^{-1}$)	V_T ($cm^3 \cdot g^{-1}$)	V_{MP} ($cm^3 \cdot g^{-1}$)
AC	756	738	18	0.45	0.39
TiO_2/AC-ST	300	110	190	0.33	0.05
TiO_2/AC-MW	323	151	172	0.38	0.07
TiO_2/AC-SG	130	115	15	0.08	0.05

S_{BET}, specific surface area; S_{MP} and S_{EXT}, microporous and non-microporous surface area; V_T and V_{MP}, total and micropore volume.

The UV-Vis DRS absorption spectra of the photocatalysts are depicted in Figure 4a. The samples show the absorption band in the UV region ($\lambda < 400$ nm) corresponding to TiO_2 and also absorb a significant amount of radiation in the visible range, due to the presence of the activated carbon support, which confers to the samples their characteristic grey color. The estimated band gaps values (E_g) were obtained from the Tauc plots (Figure 4b), considering the heterostructures as indirect semiconductors (like the bare TiO_2). Since TiO_2 is supported on a carbon material that absorbs light because of its dark color, the band gaps were estimated from the extrapolation of the linear region to the background line of the support. The respective values are included in Table 1. All the heterostructures exhibit quite similar E_g values, close to that of bare TiO_2 [27,46,47], indicating that the interaction with the AC does not modify the TiO_2 band gap in any case.

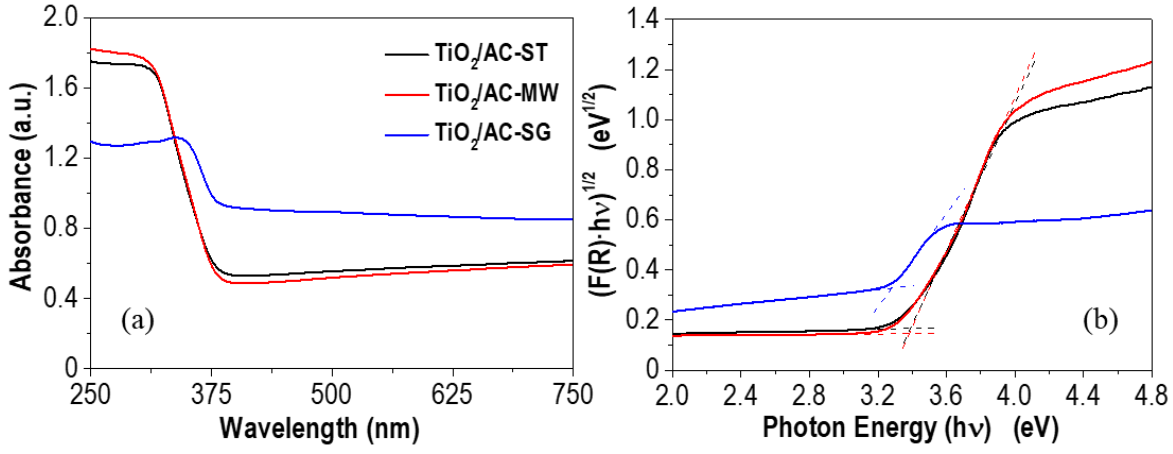

Figure 4. (a) UV–vis diffuse absorbance spectra and (b) Tauc plots of the TiO_2/AC heterostructures.

3.2. Photocatalytic performance

The different porosity and surface chemistry of the heterostructures can determine differences in the adsorption capacity. Then, prior to the photocatalytic tests, adsorption experiments with each target pollutant were carried out in dark for 16 h. This long-term stage (which can be illustrated by the pseudo second order kinetics of pharmaceutical adsorption onto the TiO_2/AC-MW heterostructure, see Table S1 and Figure S3) was performed to ensure the adsorption equilibrium of the contaminants, leading a better comparison of the photocatalytic performances. Taking into account adsorption results, the initial pollutant concentration was adjusted in order to have a liquid-phase concentration close to 5 $mg \cdot L^{-1}$ before irradiation. Thus, all the photocatalytic degradation tests were performed at almost similar starting concentrations of emerging contaminant. Figure 5 shows the evolution of ACE concentration upon irradiation time with all the TiO_2/AC heterostructures tested. A blank experiment in absence of photocatalyst was also performed, confirming that photolysis of ACE was almost negligible. TiO_2/AC-ST and TiO_2/AC-MW yielded a very similar disappearance rate of ACE, achieving almost complete conversion after 4 h under solar light, while TiO_2/AC-SG required 6 h to reach only ca. 50%. TOC removal after 6 h of reaction has been also included in Figure 5 (inset Table). TiO_2/AC-MW allowed the highest mineralization, 47%, somewhat higher than the achieved with TiO_2/AC-ST, while TiO_2/AC-SG yielded only 15% mineralization. This much poorer results with TiO_2/AC-SG can be initially associated to its higher crystal and particle size and lower porosity. Nevertheless, photocatalytic performance also depends on the transfer and recombination of the photogenerated charges. Thus, photoluminescence (PL) studies have been carried out considering that a reduction of the fluorescence intensity indicates a lower charge recombination rate. The resulting PL spectra are depicted in Figure 6. As can be seen, there are no major differences among the three heterostructures, just mention that the TiO_2/AC-MW spectrum has a slightly low intensity than that described by TiO_2/AC-ST. But the difference is very small, suggesting that the photoactivity is fundamentally controlled by the structural and textural properties. The results so far show that the sol-gel route, although it is conventionally used for the synthesis of TiO_2 heterostructures, does not seem to be the most appropriate looking at the photocatalytic performance of the resulting material. The microwave-assisted route appears as the best synthesis way in that respect.

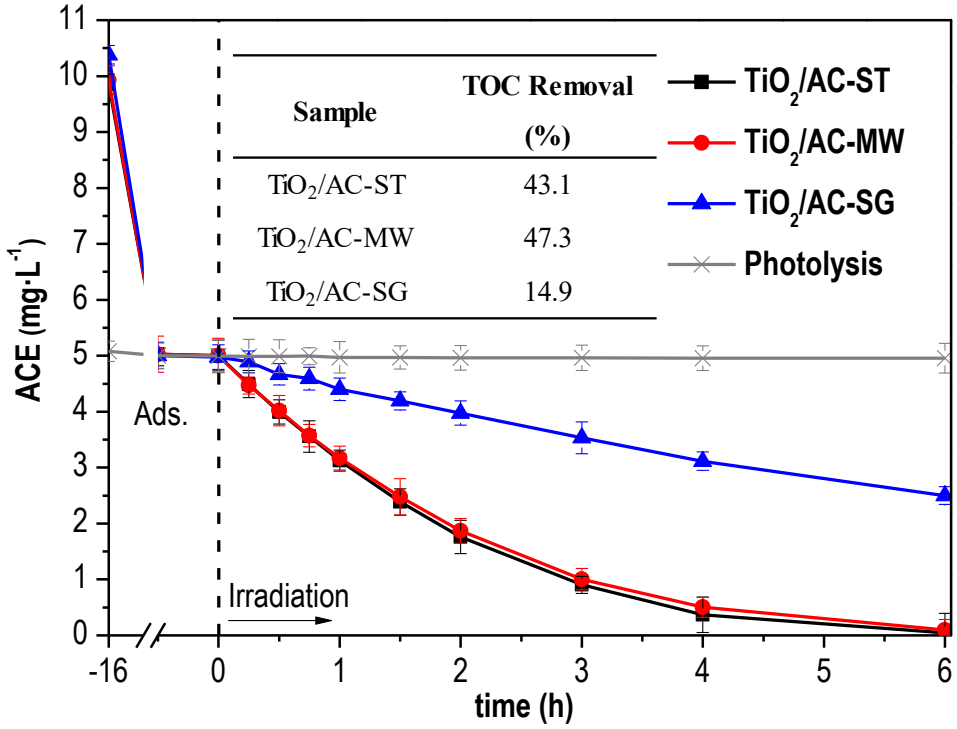

Figure 5. Time course of ACE concentration under solar irradiation with the heterostructures tested ([Photocatalyst]$_0$: 250 mg·L^{-1} of TiO_2; Intensity of irradiation: 600 W·m^{-2}).

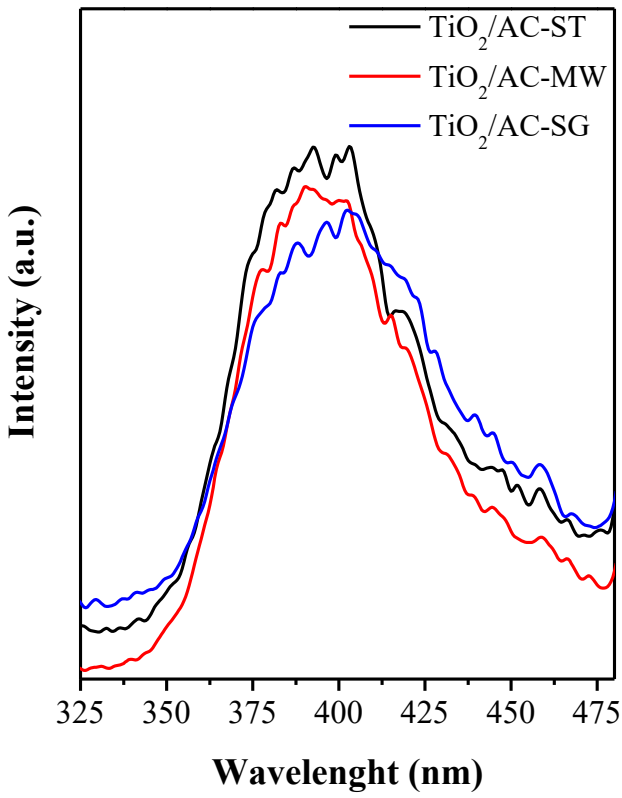

Figure 6. Photoluminescence spectra (PL) of the TiO_2/AC heterostructures.

Table 3 summarizes the values of the pseudo-first order rate constant of ACE disappearance with these materials and other heterostructures reported in previous works, all of them under solar light. The highest values obtained in the current study (ca. 0.50 h^{-1}) were significantly higher than the reported for ZnO/sepiolite [48], although somewhat lower than the corresponding to other TiO_2–based photocatalysts [49–52].

Table 3. Values of the first order kinetic constant, (h^{-1}), of ACE disappearance under solar light with this and other work materials.

Photocatalyst		Reference
TiO_2/AC-ST	0.50	This work
TiO_2/AC-MW	0.47	This work
TiO_2/AC-SG	0.11	This work
ZnO/sepiolite	0.19	[48]
Zr-doped TiO_2/clay	0.59	[49]
TiO_2(P25)/cellulosic fibers	0.61	[51]
Ag/ZnO-TiO_2/clay	0.57	[52]

Figure 7 depicts the evolution of IBU and ANT concentration upon photocatalytic degradation with TiO_2/AC-ST and TiO_2/AC-MW under solar irradiation (TiO_2/AC-SG was discarded due to its significantly lower photocatalytic performance). Both heterostructures allowed almost complete IBU conversion in less than 3 h, while that was not achieved for ANT even after 6 h. TiO_2/AC-MW exhibited somewhat higher photocatalytic activity with both pharmaceuticals. The inset Tables show the higher mineralization achieved with this last catalyst, being the difference significantly more pronounced for the degradation of ANT. Table 4 collects the values of the corresponding first order disappearance rate constant. Values previously reported with other photocatalysts have been also included for the sake of comparison. In the case of IBU the two heterostructures of the current work provided significantly faster degradation but the opposite was observed with ANT. It is noteworthy that the photocatalytic activity of ~~the~~ TiO_2/AC-MW depends on the nature of the target compound used. Comparing the results of Figures 5 and 7, and Tables 3 and 4, it appears that IBU is more easily degraded than ACE and the latter more than ANT. Considering the chemical structure of these pharmaceuticals (included in Figure S1 at Supplementary Information), it appears that

nitrogenous compounds are more refractory, being much more evident for ANT due to its pyrazolone group.

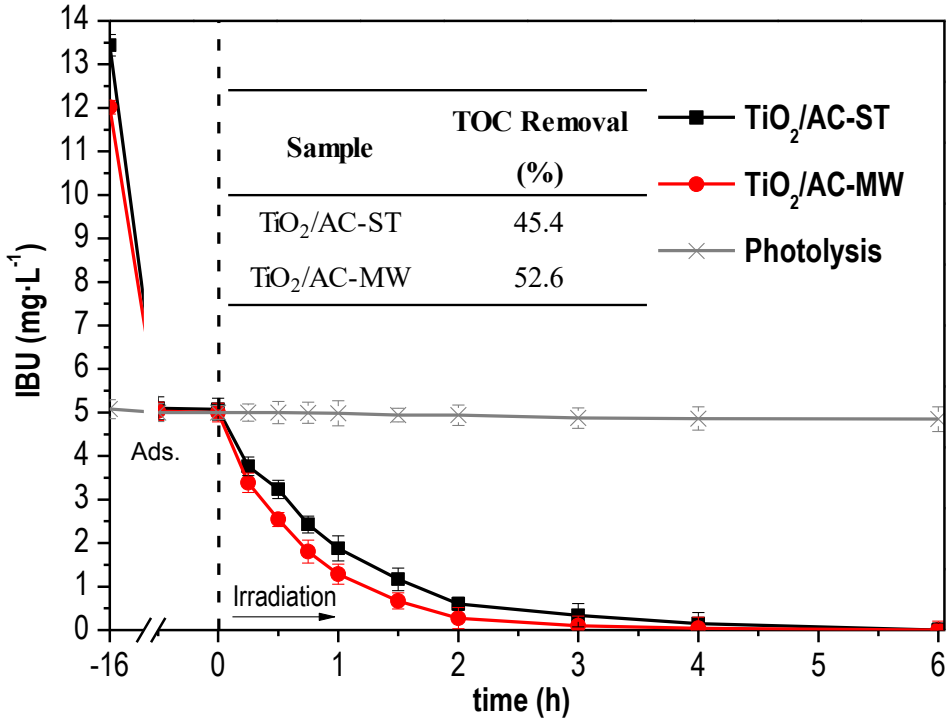

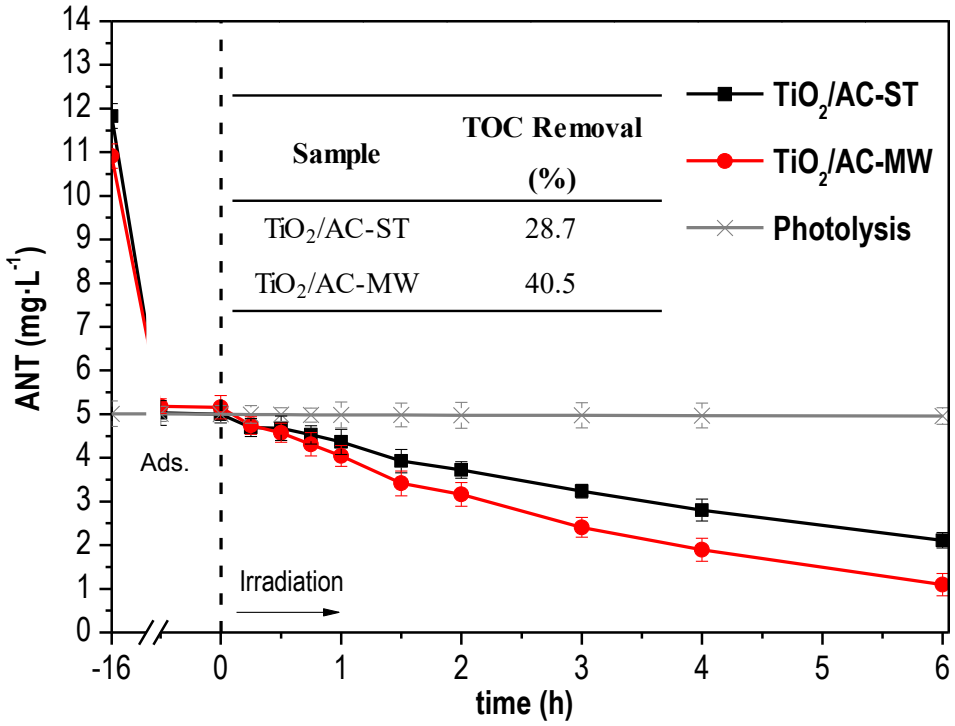

Figure 7. Time-course of IBU and ANT concentration upon solar photocatalytic degradation with the heterostructures tested. Operating conditions as in Figure 5.

Table 4. Values of the first order rate constant, (h^{-1}), of IBU and ANT disappearance under solar light with this and other works photocatalysts.

Photocatalyst	IBU	ANT	Reference
TiO_2/AC-ST	1.10	0.15	This work
TiO_2/AC-MW	1.40	0.25	This work
ZnO/sepiolite	0.38	0.13	[48]
Zr-doped TiO_2/clay	n.d.	0.58	[49]
Ag/ZnO-TiO_2/clay	n.d.	0.55	[52]
TiO_2	0.60	n.d.	[53]
ZnFe-MMOs	0.95	n.d.	[54]

n.d.: no data.

The TiO_2/AC-MW catalyst, the one giving the best results with each individual target compound was tested with a mixture of them. In this case, the initial concentration of each species was fixed at the same value of 5 $mg \cdot L^{-1}$ before the dark-adsorption step and so, different concentrations were remaining in solution at the start of solar irradiation, i.e., the photocatalytic stage. Figure 8 shows the results of this experiment. Firstly, very significant differences can be seen regarding the amount adsorbed of each target compound prior to the reaction, following the order ACE>>ANT>IBU. This order does not correspond with the expected from the previously observed in the single-compound experiments. Thus, competitive adsorption has a dramatic effect on the uptake of the individual species. Regarding photocatalytic conversion, the rate of disappearance is quite similar to the observed in the respective individual experiments, according to the values of the first-order rate constant (see Tables 3-5). Close to 50% mineralization was achieved after 6 h. An additional test was carried out using longer times, up to 24 h (Figure S4 of Supplementary Information), but, although almost complete conversion of the three target compounds was achieved, the TOC reduction remained almost unchanged, close to 50%, indicating the existence of degradation byproducts refractory to this treatment. In fact, it must also be considered that some byproducts can be adsorbed on the catalyst surface, which would lead a decrease of the mineralization rate.

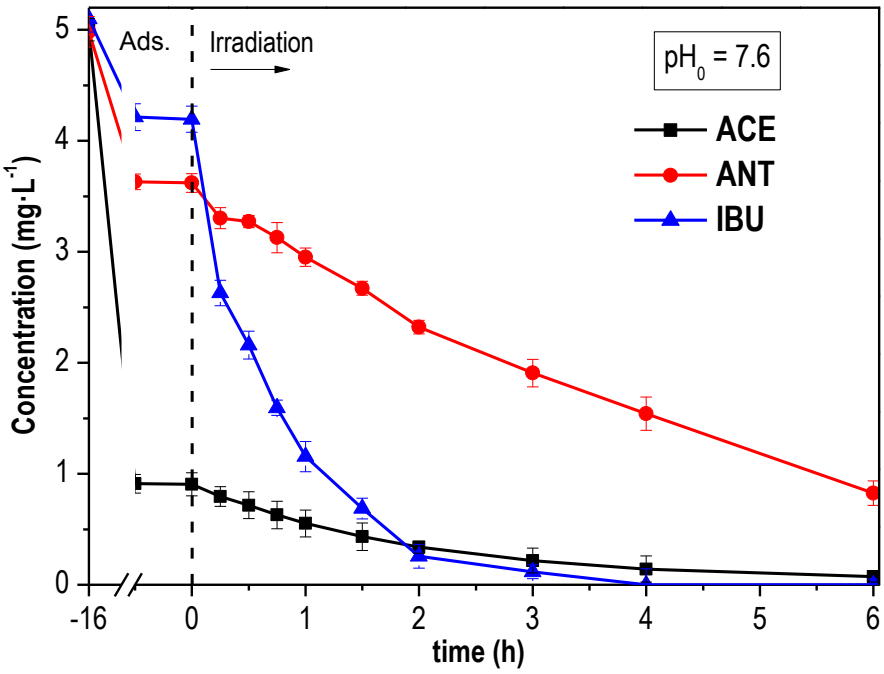

Figure 8. Adsorption and solar photocatalytic degradation of ACE, IBU and ANT with TiO_2/AC-MW (250 mg·L^{-1} of TiO_2) from an aqueous solution of the three compounds (Intensity of irradiation: 600 W·m^{-2}).

Table 5. Values of the first order rate constant, (h^{-1}), of disappearance and TOC removal after 6 h from the experiments of Figure 8 and 9.

Initial pH	ACE	IBU	ANT	TOC removal (%)
3	0.37	--	1.00	23.3
5	0.39	--	0.81	41.5
7.6	0.49	1.33	0.23	48.8
9	0.72	1.00	0.37	42.3
11	0.88	0.53	0.32	16.9

Similar experiments to those of Figure 8 were repeated at different initial pH values. The results are depicted in Figure 9. As can be seen, this variable affected significantly to both adsorption and photocatalytic degradation. At the starting concentration used, IBU was almost completely removed from solution by adsorption at pH ≤ 5. At alkaline pH adsorption decreases because of the electrostatic repulsion between the anionic IBU species (pK_a=4.4) and the catalyst surface (pH_{pzc}=7.0, Figure S5 of Supplementary

Information). Of course, adsorption is not only determined by electrostactic forces but dispersive interactions can be also important depending on the structure of the adsorbate and taking into account, among other, donor-acceptor mechanisms involving π electrons of the aromatic ring of the target compounds (in this case) as well as of the graphene-like layers of activated carbon. That complex force-balance could explain some discontinuities observed in the evolution of adsorption vs pH, moreover, taking also into account the occurrence of competitive adsorption. The size and conformation of the target compound can also influence the adsorption capacity considering the essentially microporous texture of the AC component of the heterostructure. Information on the chemical structure and 3D conformation of the three pharmaceuticals has been included in Supplementary Information (Figure S1). ACE is a p-aminophenol derivative with a planar configuration [55], IBU is a propionic acid derivative with a flexible configuration due to the presence of several torsional twists [56] and ANT is a pyrazolone derivative with a coplanar configuration [57]. Apparently, the flexibility of the IBU favors its adsorption on the surface of the catalyst. Regarding the photocatalytic performance of TiO_2/AC-MW for the degradation of pharmaceuticals mixture at different initial pH, Table 5 collects the values of the first order kinetic constant describing the rate of disappearance of each pharmaceutical and the overall TOC removal after 6 h of solar irradiation. As can be seen ANT undergoes faster and complete conversion at low initial pH values while ACE degradation is favored at high pH. IBU shows the highest degradation rate at medium pH, but its almost complete adsorption at low pH impeded learning on its photocatalytic degradation at these low pH values.

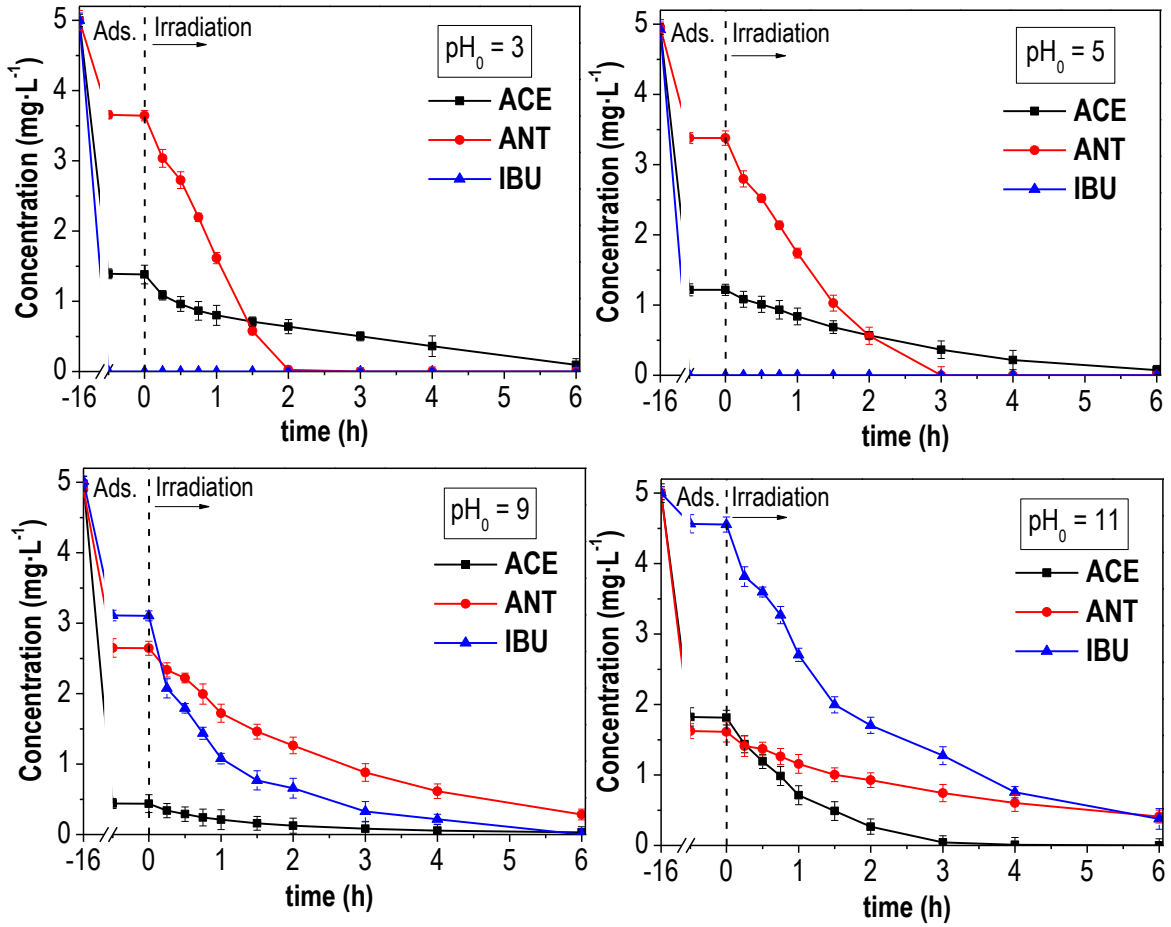

Figure 9. Adsorption and solar photocatalytic degradation of ACE, IBU and ANT with TiO_2/AC-MW at different initial pH values from aqueous solution of the three compounds.

3.3. Photocatalytic intermediates and degradation pathway

The intermediate products in the photocatalytic degradation pathways of the three pharmaceuticals (individual experiments at initial concentration of 100 $mg \cdot L^{-1}$ and pH ≈7) using TiO_2/AC-MW were identified by LC/ESI-MS and IC. The accurate mass of the intermediates are listed, with the corresponding proposed compounds, in Tables S2-4 of the Supplementary Information. The assessment of the chemical species can be considered highly confident taking into account the low mass error (mainly < ±1 mDa) and the value of ring and double bond (RDB). This last parameter corresponds to the number of rings and double bonds existing in a molecule (e.g., parent ACE has a RDB of 5, attributed to the aromatic ring (3 correspond to the double bonds and 1 to the ring) and the double bond C=O in the acetamide group).

For ACE photodegradation, the peaks detected and their proposed identification are collected in Table S2 and the feasible degradation pathways are shown in Figure 10. The ring opening of ACE results in the formation of ACE-1 (protonated form with m/z 118.0857, see Table S2) and succinic and malonic acids. The presence of these acids was also observed in previous studies [59,61,62]. Further oxidation and mineralization of these intermediates lead the formation of acetic and formic acids, and finally CO_2, NO_3^- and H_2O. In addition, the evolution of the short-chain carboxylic acids and NO_3^- has been included in the Supplementary Information (Figure S6a). It can be observed the rapid appearance of succinic acid in the first 15 min of photocatalytic treatment, which disappears along the reaction time, giving rise to the formation of other short-chain acids. It is important to remark that nitrite (NO_2^-) was never detected, being only nitrate (NO_3^-) the resulting mineralized product from the N-C moiety of the initial ACE. Other intermediates identified are derived from the coupling of ACE. Two isomers of ACE-2 (m/z 301.1179) coupling product have been detected, as previously reported by Chen et al. [63], whose photodegradation derived on other products following up to three different pathways: i) the loss of one of the acetamide groups followed by hydroxylation, leading to the formation of ACE-3 (m/z 260.0914); ii) direct aromatic ring hydroxylation, giving rise to the detected intermediates ACE-4 and ACE-5 (m/z 317.1130 and 349.1029, respectively); and iii) further coupling reaction leading to ACE-6 (m/z 450.1653), being identified 3 isomers. The resistance to photocatalytic oxidation of these coupled products can explain the slight reduction of TOC observed in the long-term photocatalytic process (Figure S4). Unlike other reported works dealing with ACE degradation, no products derived from the direct hydroxylation of the ACE aromatic ring were identified (e.g., hydroquinone) [58–61].

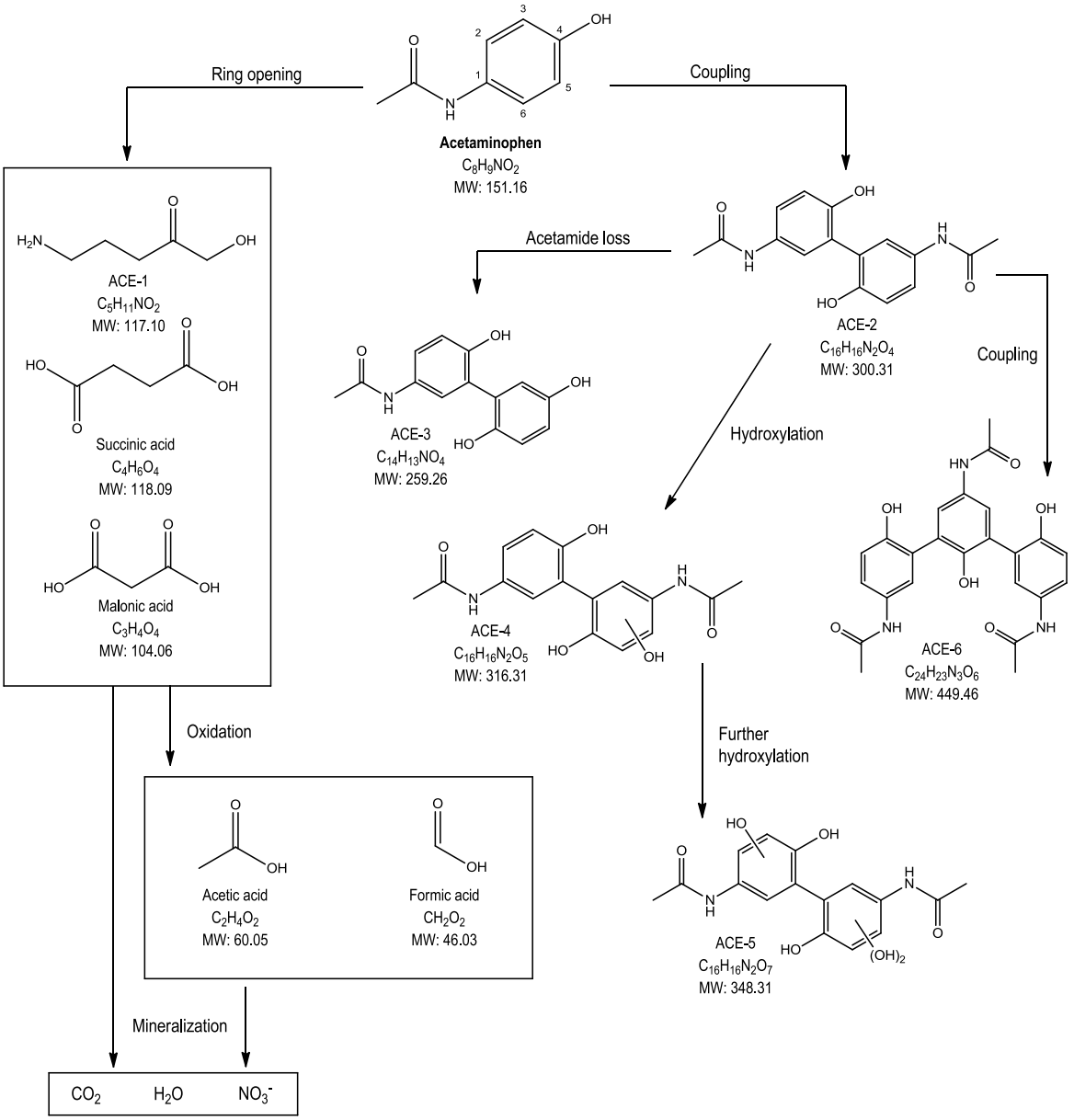

Figure 10. Proposed pathways for solar photocatalytic degradation of ACE with TiO_2/AC-MW.

In contrast to ACE, no coupled intermediates were observed in the degradation pathways of IBU (Figure 11 and Table S3). The hydroxylation of the parent IBU has been the most common oxidative process reported in literature [64–67]. A first degradation pathway can be illustrated through the hydroxylation of ^{7}C in the original structure, resulting in the formation of monohydroxylated ibuprofen [66], identified as IBU-1 (m/z 221.1191, highlights that the ionization for IBU was in negative mode). According to the previous work of Tanveer et al. [67] and Lei et al. [68], the decarboxylation of ^{11}C in IBU-1 is expected to result in the formation of IBU-1* (1-(4-ethyl-phenyl)-2-methyl-propan-1-ol;

m/z 177.1285), which was not detected in our work. However, the product from demethylation of ^{8}C in IBU-1* was identified as IBU-2 (m/z 161.0980), as well as two isomers of IBU-3 (m/z 133.0666), after dealkylation of ^{7}C in IBU-2. A previous toxicity assessment was performed by Da Silva et al.[69], showing that these ibuprofen photocatalytic degradation intermediates had lower ecotoxicity in *Artemia salina* than the parent pharmaceutical. Finally, the IC results showed that the ring cleavage of these compounds leads to the formation of the short-chain carboxylic acids, namely succinic, malonic, acetic and formic. As can be observed in Figure S6b, the concentration of formic acid in the case of IBU degradation was the highest detected from the three pharmaceuticals after 6 h under simulated solar light, consistent with the higher removal of this compound compared to the other two contaminants tested. Further oxidation leads to, CO_2 and H_2O. Ibuprofen can be also degraded by the opening of the phenyl ring, giving IBU-4 (m/z 237.1142). It has to be remarked that this reaction intermediate has not been previously identified in the literature. In addition, the oxidation of the –CHO groups in this intermediate after the ring cleavage results in IBU-5 (m/z 269.1043), which can be further oxidized up to short-chain carboxylic acids, as previously indicated. According to the results of the LC/ESI-MS spectrometry, a third degradation route can be proposed for the original ibuprofen, consisting in a first demethylation of the ^{8}C, giving IBU-6 (m/z 191.1086). Then, a second dealkylation step of the ^{3}C leads to the formation of IBU-7 (m/z 149.0616), which upon further ring opening can also yield ~~to~~ short-chain carboxylic acids, further mineralized.

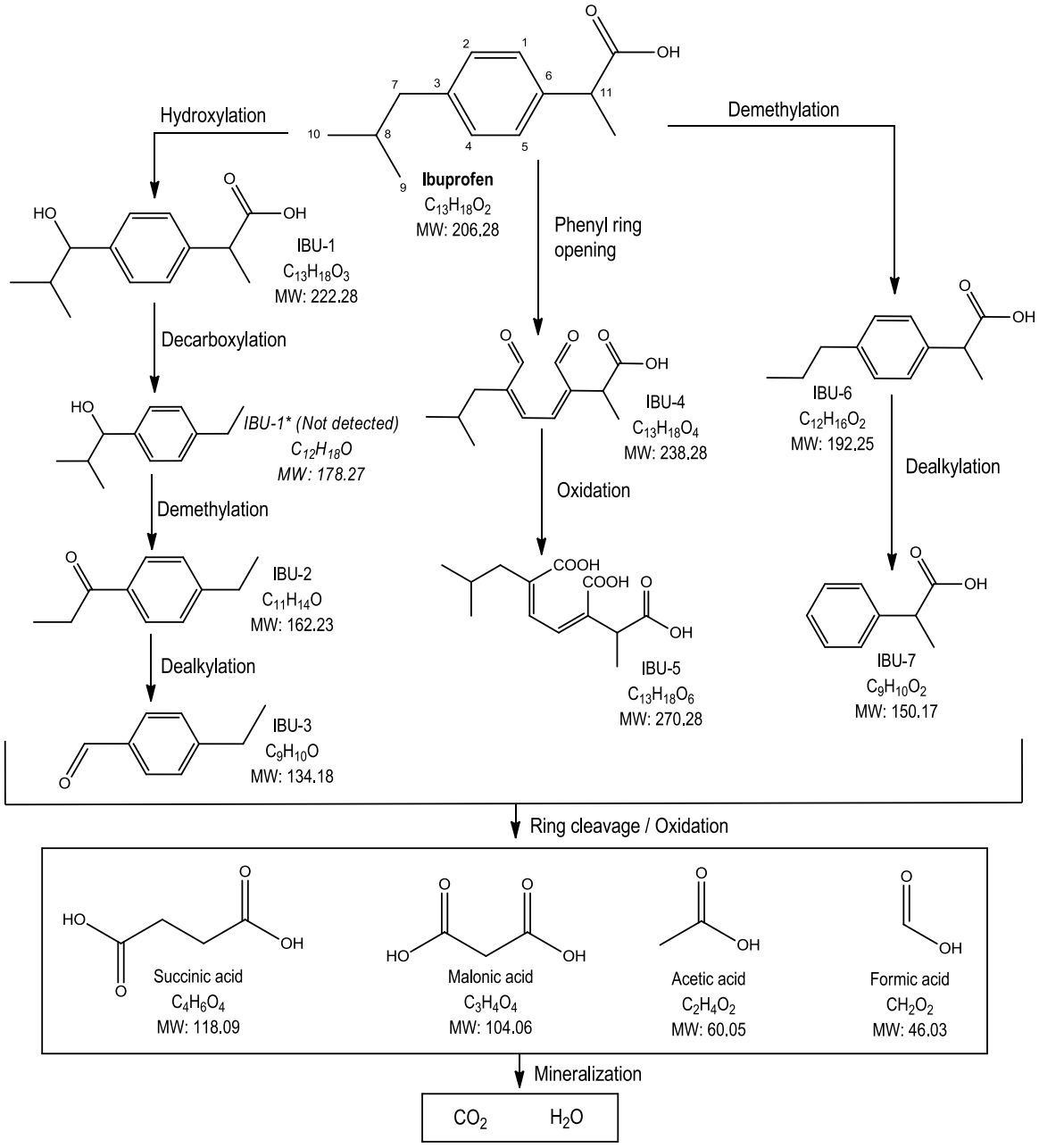

Figure 11. Proposed degradation pathways for solar photocatalytic degradation of IBU with TiO_2/AC-MW.

The proposed photocatalytic degradation pathways of the third pharmaceutical tested in this work, ANT, are shown in Figure 12 (and the identified intermediates listed in Table S4). Three degradation routes are proposed also in this case. In the first one, the loss of the phenyl ring gives rise to the formation of ANT-1 (m/z 113.0689). This compound results from the break of the ^{1}N-^{6}C bond and can be further oxidized to succinic, acetic and formic acids and subsequently to final mineralization products (CO_2, H_2O and NO_3^-) after opening of the pyrazole ring. The evolution of the short-chain carboxylic acids can be

followed in Figure S6c, where it can be seen a different route for the removal of succinic acid compared to that in the case of ACE and IBU. The lower degradation of succinic acid can be one of the possible reasons of the lower TOC removal observed for ANT compared to the other two pharmaceuticals (as previously seen in Figures 5 and 7). On the other hand, and as in the case of ACE, no nitrite was detected in the IC chromatograms. In the second degradation pathway proposed, the cleavage of the pyrazole ring leads to the formation of ANT-2 (m/z 221.0917), which can be degraded by two different ways. On the one hand, through the loss of the oxamoyl chain, giving ANT-3 (m/z 165.1018), as previously reported by Miao et al. [70]. In our current study, a further degradation compound, after double methylation, was observed, listed as ANT-4 (m/z 137.0706). On the other hand, through hydroxylation of the –CHO group in ANT-2, leading to the formation of ANT-5 (m/z 237.0867). In addition, this intermediate can yield the previously indicated ANT-3, after the loss of the 2-oxoacetic acid group in ^{1}N. The third route for the degradation of the parent antipyrine consists of its mono-hydroxylation [70,71]. In the degradation pathway described in the current work, if the hydroxylation of parent ANT occurs in the ^{4}C, ANT-6 (m/z 205.0967) could be formed, which can result in ANT-5 by the cleavage of the pyrazole ring. Moreover, that can also allow the formation of ANT-7 (m/z 393.1559), by coupling of two ANT-6 molecules. In contrast, if the hydroxylation takes place in the aromatic ring of the original ANT, that can lead to 3 isomer structures (ANT 8, m/z 205.0963). Further hydroxylation on ANT-8 would result in the formation of ANT-9 (m/z 221.0917). The oxidation of the listed intermediates leads to the formation of short-chain acids and mineralized products, as previously commented. It has to be remarked that, unlike other degradation pathways of antipyrine found in literature [72–74], anthranilic or 1,4-benzenedicarboxylic acids were not detected.

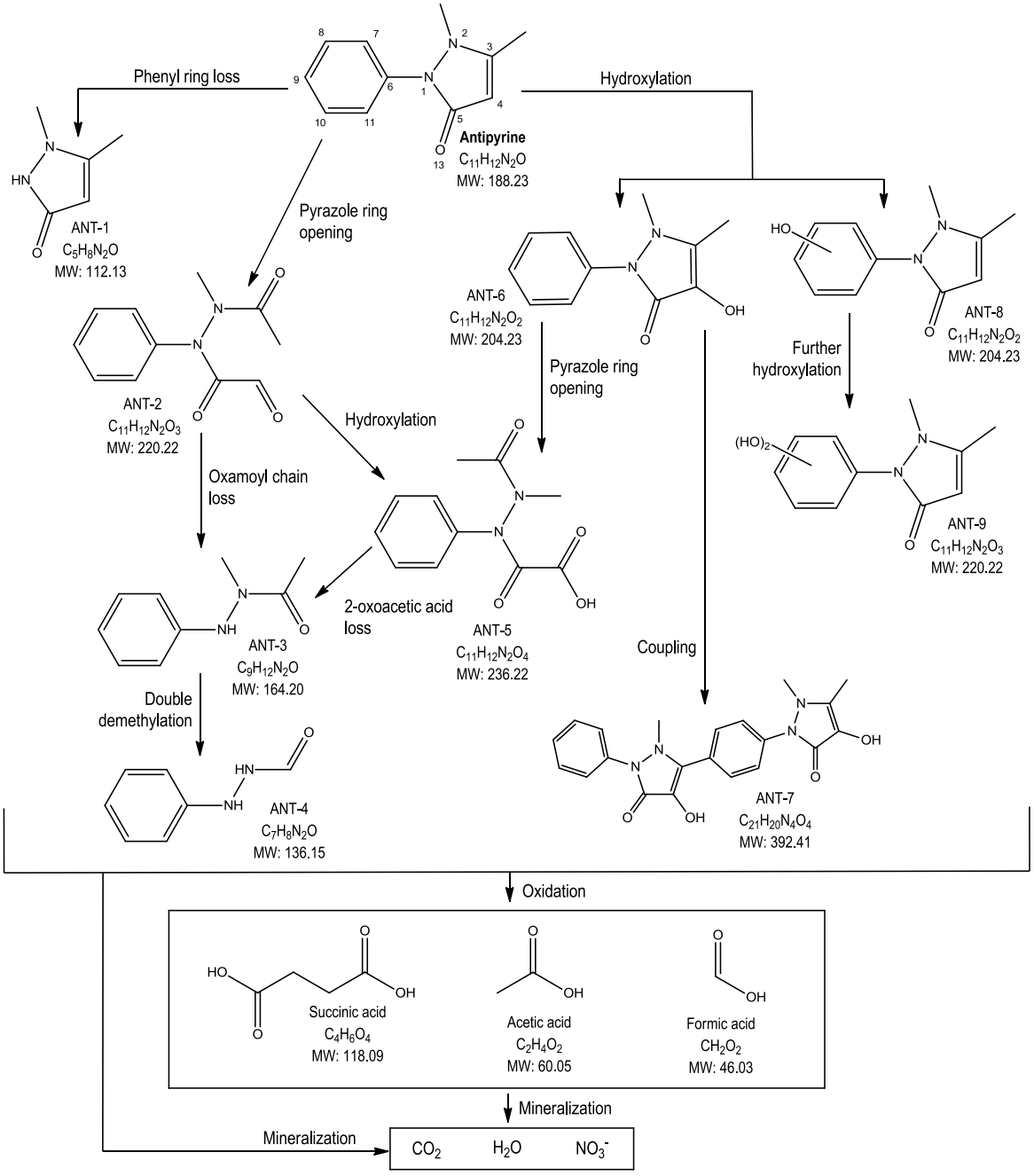

Figure 12. Proposed pathways for solar photocatalytic degradation of ANT with TiO_2/AC-MW.

4. Conclusions

Heterostructures based on TiO_2 supported on activated carbon (TiO_2/AC) have been successfully synthesized through three different procedures (solvothermal, microwave-assisted and sol-gel), using lignin as carbonaceous precursor. All the heterostructures contained anatase as the only crystalline phase. TiO_2/AC-ST and TiO_2/AC-MW samples

have similar properties, characterized by a predominantly mesoporous texture but with significant contribution of microporosity basically associated to the AC component. They are characterized by low TiO_2 crystal size (10 nm) and mean particle size close to 0.25 μm, with a band gap ranging within 3.28-3.38 eV, close to that of bare TiO_2. The heterostructure synthesized by a sol-gel route showed some slight differences, such as higher crystal and particle sizes and lower surface area, most probably due to the higher temperature reached during the heat-treatment included in this synthesis route to achieve anatase crystallization. Regarding the photocatalytic activity, the heterostructure synthesized by a microwave-assisted route (TiO_2/AC-MW) yielded the best performance in the solar-driven photocatalytic degradation of the three pharmaceuticals tested (ACE, IBU and ANT), both in terms of parent compound disappearance (conversion) and mineralization. The best results were obtained for IBU degradation, with complete conversion in less than 3 h, while ANT was found the most recalcitrant.

The degradation pathways proposed for ACE suggest a rapid ring opening leading to the mineralization products (CO_2, H_2O and NO_3^-). However, this mineralization is affected by the generation of coupled intermediates. In the case of IBU, its degradation takes place ~~is~~ mainly through hydroxylation and dealkylation reactions, giving rise to easier ring cleavage to form short-chain carboxylic acids and further mineralization products. Meanwhile, the degradation route for ANT involves a fast opening of the pyrazole ring instead of the phenyl one, in parallel to hydroxylation of the original structure of ANT and the formation of coupled byproducts with apparent high resistance to photocatalytic oxidation.

The performance of TiO_2/AC-MW was also evaluated with a mixture of the three pharmaceuticals at different initial pH values. The highest disappearance rate and overall TOC removal occurred at pH between 7 and 9. Microwave-assisted synthesis can be considered a fast and simple route for preparing heterostructures with promising photocatalytic activity for the abatement of these CECs under solar light.

Supplementary Information

Table S1. Kinetic modelling results of the pseudo-first and second order adsorption of the three contaminants on TiO_2/AC-MW heterostructure.

Table S2. Accurate mass (m/z) values obtained for ACE and its proposed photocatalytic degradation products with the TiO_2/AC-MW heterostructure.

Table S3. Accurate mass (m/z) values obtained for IBU and its proposed photocatalytic degradation products with the TiO_2/AC-MW heterostructure.

Table S4. Accurate mass (m/z) values obtained for ANT and its proposed photocatalytic degradation products with the TiO_2/AC-MW heterostructure.

Figure S1. Chemical structure and 3D conformation of acetaminophen, ibuprofen and antipyrine, from PubChem open chemistry database, National Institutes of Health (NIH).

Figure S2. Low-magnification SEM images of (a) TiO_2/AC-ST, (b) TiO_2/AC-MW and (c) TiO_2/AC-SG.

Figure S3. Experimental adsorption data of the different contaminants on TiO_2/AC-MW heterostructure.

Figure S4. Conversion values for TOC, ACE, IBU and ANT with TiO_2/AC-MW at pH 7.6 from aqueous solution of the three compounds at different irradiation times.

Figure S5. Determination of pH_{pzc} for TiO_2/AC-ST and TiO_2/AC-MW.

Figure S6. Evolution of short-chain organic acids and nitrate (NO_3^-) concentration upon solar photocatalytic degradation with TiO_2/AC-MW of: a) ACE, b) IBU, c) ANT. (Initial concentration of each pharmaceutical = 100 $mg \cdot L^{-1}$).

Acknowledgements

The authors acknowledge the financial support from Spanish MINECO (project CTQ2016-78576-R). M. Peñas-Garzón thanks Spanish MECD for FPU16/00576 grant. Authors thank the Research Support Services of the University of Extremadura (SAIUEx) for its technical and scientific support.

References

[1] Y. Yang, Y.S. Ok, K.H. Kim, E.E. Kwon, Y.F. Tsang, Occurrences and removal of pharmaceuticals and personal care products (PPCPs) in drinking water and water/sewage treatment plants: A review, Sci. Total Environ. 596–597 (2017) 303–320. doi:10.1016/j.scitotenv.2017.04.102.

[2] S.D. Richardson, T.A. Ternes, Water Analysis: Emerging Contaminants and Current Issues, Anal. Chem. 90 (2018) 398–428. doi:10.1021/acs.analchem.7b04577.

[3] S. Mompelat, B. Le Bot, O. Thomas, Occurrence and fate of pharmaceutical products and by-products, from resource to drinking water, Environ. Int. 35 (2009) 803–814. doi:10.1016/j.envint.2008.10.008.

[4] M. Papageorgiou, C. Kosma, D. Lambropoulou, Seasonal occurrence, removal, mass loading and environmental risk assessment of 55 pharmaceuticals and personal care products in a municipal wastewater treatment plant in Central Greece, Sci. Total Environ. 543 (2016) 547–569. doi:10.1016/j.scitotenv.2015.11.047.

[5] N.A. Alygizakis, P. Gago-Ferrero, V.L. Borova, A. Pavlidou, I. Hatzianestis, N.S. Thomaidis, Occurrence and spatial distribution of 158 pharmaceuticals, drugs of abuse and related metabolites in offshore seawater, Sci. Total Environ. 541 (2016) 1097–1105. doi:10.1016/j.scitotenv.2015.09.145.

[6] J.C.G. Sousa, A.R. Ribeiro, M.O. Barbosa, M.F.R. Pereira, A.M.T. Silva, A review on environmental monitoring of water organic pollutants identified by EU guidelines, J. Hazard. Mater. 344 (2018) 146–162. doi:10.1016/j.jhazmat.2017.09.058.

[7] S. Sifakis, V.P. Androutsopoulos, A.M. Tsatsakis, D.A. Spandidos, Human exposure to endocrine disrupting chemicals: effects on the male and female reproductive systems, Environ. Toxicol. Pharmacol. 51 (2017) 56–70. doi:10.1016/j.etap.2017.02.024.

[8] A. Durán, J.M. Monteagudo, I. San Martín, Operation costs of the solar photo-catalytic degradation of pharmaceuticals in water: A mini-review, Chemosphere. 211 (2018) 482–488. doi:10.1016/j.chemosphere.2018.07.170.

[9] T. Deblonde, C. Cossu-Leguille, P. Hartemann, Emerging pollutants in wastewater: A review of the literature, Int. J. Hyg. Environ. Health. 214 (2011) 442–448. doi:10.1016/j.ijheh.2011.08.002.

[10] U.N.G. Assembly, Transforming our world: the 2030 Agenda for Sustainable Development, 2015. https://www.unfpa.org/sites/default/files/resource-pdf/Resolution_A_RES_70_1_EN.pdf (accessed April 10, 2019).

[11] L. Rizzo, S. Malato, D. Antakyali, V.G. Beretsou, M.B. Đolić, W. Gernjak, E. Heath, I. Ivancev-Tumbas, P. Karaolia, A.R. Lado Ribeiro, G. Mascolo, C.S. McArdell, H. Schaar, A.M.T. Silva, D. Fatta-Kassinos, Consolidated vs new advanced treatment methods for the removal of contaminants of emerging concern from urban wastewater, Sci. Total Environ. 655 (2019) 986–1008. doi:10.1016/j.scitotenv.2018.11.265.

[12] Z. Cai, A.D. Dwivedi, W.-N. Lee, X. Zhao, W. Liu, M. Sillanpää, D. Zhao, C.-H. Huang, J. Fu, Application of nanotechnologies for removing pharmaceutically active compounds from water: development and future trends, Environ. Sci. Nano. 5 (2018) 27–47. doi:10.1039/C7EN00644F.

[13] C. Byrne, G. Subramanian, S.C. Pillai, Recent advances in photocatalysis for environmental applications, J. Environ. Chem. Eng. 6 (2018) 3531–3555. doi:10.1016/j.jece.2017.07.080.

[14] H. Dong, G. Zeng, L. Tang, C. Fan, C. Zhang, X. He, Y. He, An overview on limitations of TiO2-based particles for photocatalytic degradation of organic pollutants and the corresponding countermeasures, Water Res. 79 (2015) 128–146. doi:10.1016/j.watres.2015.04.038.

[15] B. Srikanth, R. Goutham, R. Badri Narayan, A. Ramprasath, K.P. Gopinath, A.R. Sankaranarayanan, Recent advancements in supporting materials for immobilised photocatalytic applications in waste water treatment, J. Environ. Manage. 200 (2017) 60–78. doi:10.1016/j.jenvman.2017.05.063.

[16] C. Belver, J. Bedia, J.J. Rodriguez, Titania-clay heterostructures with solar photocatalytic applications, Appl. Catal. B Environ. 176–177 (2015) 278–287. doi:10.1016/j.apcatb.2015.04.004.

[17] F.J. García-Mateos, R. Berenguer, M.J. Valero-Romero, J. Rodríguez-Mirasol, T. Cordero, Phosphorus functionalization for the rapid preparation of highly nanoporous submicron-diameter carbon fibers by electrospinning of lignin solutions, J. Mater. Chem. A. 6 (2018) 1219–1233. doi:10.1039/c7ta08788h.

[18] F. García-Mateos, I. Moulefera, J. Rosas, A. Benyoucef, J. Rodríguez-Mirasol, T. Cordero, Alcohol Dehydrogenation on Kraft Lignin-Derived Chars with Surface Basicity, Catalysts. 7 (2017) 308. doi:10.3390/catal7100308.

[19] D.A. Baker, T.G. Rials, Recent advances in low-cost carbon fiber manufacture from lignin, J. Appl. Polym. Sci. 130 (2013) 713–728. doi:10.1002/app.39273.

[20] J.M. Rosas, R. Berenguer, M.J. Valero-Romero, J. Rodríguez-Mirasol, T. Cordero, Preparation of Different Carbon Materials by Thermochemical Conversion of Lignin, Front. Mater. 1 (2014) 1–17. doi:10.3389/fmats.2014.00029.

[21] R. Ruiz-Rosas, J. Bedia, M. Lallave, I.G. Loscertales, A. Barrero, J. Rodríguez-Mirasol, T. Cordero, The production of submicron diameter carbon fibers by the electrospinning of lignin, Carbon N. Y. 48 (2010) 696–705. doi:10.1016/j.carbon.2009.10.014.

[22] F.J. García-Mateos, T. Cordero-Lanzac, R. Berenguer, E. Morallón, D. Cazorla-Amorós, J. Rodríguez-Mirasol, T. Cordero, Lignin-derived Pt supported carbon (submicron)fiber electrocatalysts for alcohol electro-oxidation, Appl. Catal. B Environ. 211 (2017) 18–30. doi:10.1016/j.apcatb.2017.04.008.

[23] C. Fernandez-Ruiz, J. Bedia, P. Bonal, J.J. Rodriguez, L.M. Gómez-Sainero, Chloroform conversion into ethane and propane by catalytic hydrodechlorination with Pd supported on activated carbons from lignin, Catal. Sci. Technol. 8 (2018) 3926–3935. doi:10.1039/C8CY00461G.

[24] J.M. Rosas, R. Ruiz-Rosas, J. Rodríguez-Mirasol, T. Cordero, Kinetic study of SO_2 removal over lignin-based activated carbon, Chem. Eng. J. 307 (2017) 707–721. doi:10.1016/j.cej.2016.08.111.

[25] J.J. Rodríguez, T. Cordero, J. Rodríguez-Mirasol, Carbon Materials from Lignin and Their Applications, Biofuels and Biorefineries. 6 (2016). doi:10.1007/978-981-10-1965-4_8.

[26] Suhas, P.J.M. Carrott, M.M.L. Ribeiro Carrott, Lignin - from natural adsorbent to activated carbon: A review, Bioresour. Technol. 98 (2007) 2301–2312. doi:10.1016/j.biortech.2006.08.008.

[27] M. Peñas-Garzón, A. Gómez-Avilés, J.B. Garcia-Matamoros, J.J. Rodriguez, C. Belver, Effect of Activating Agent on the Properties of TiO_2/Activated Carbon Heterostructures for Solar Photocatalytic Degradation of Acetaminophen, Materials (Basel). (2019). doi:10.3390/ma12030378.

[28] D. Awfa, M. Ateia, M. Fujii, M.S. Johnson, C. Yoshimura, Photodegradation of pharmaceuticals and personal care products in water treatment using carbonaceous-TiO2 composites: A critical review of recent literature, Water Res. 142 (2018) 26–45. doi:10.1016/j.watres.2018.05.036.

[29] A. Rey, D.H. Quiñones, P.M. Álvarez, F.J. Beltrán, P.K. Plucinski, Simulated solar-light assisted photocatalytic ozonation of metoprolol over titania-coated magnetic activated carbon, Appl. Catal. B Environ. 111–112 (2012) 246–253. doi:10.1016/j.apcatb.2011.10.005.

[30] S.X. Liu, X.Y. Chen, X. Chen, A TiO2/AC composite photocatalyst with high activity and easy separation prepared by a hydrothermal method, J. Hazard. Mater. 143 (2007) 257–263. doi:10.1016/j.jhazmat.2006.09.026.

[31] A. Omri, S.D. Lambert, J. Geens, F. Bennour, M. Benzina, Synthesis, surface characterization and Photocatalytic activity of TiO2 supported on Almond shell

activated carbon, J. Mater. Sci. Technol. 30 (2014) 894–902. doi:10.1016/j.jmst.2014.04.007.

[32] C. Orha, R. Pode, F. Manea, C. Lazau, C. Bandas, Titanium dioxide-modified activated carbon for advanced drinking water treatment, Process Saf. Environ. Prot. 108 (2017) 26–33. doi:10.1016/j.psep.2016.07.013.

[33] J. Bedia, C. Belver, S. Ponce, J. Rodriguez, J.J. Rodriguez, Adsorption of antipyrine by activated carbons from FeCl3-activation of Tara gum, Chem. Eng. J. 333 (2018) 58–65. doi:10.1016/j.cej.2017.09.161.

[34] J. Bedia, V.M. Monsalvo, J.J. Rodriguez, A.F. Mohedano, Iron catalysts by chemical activation of sewage sludge with FeCl3for CWPO, Chem. Eng. J. 318 (2017) 224–230. doi:10.1016/j.cej.2016.06.096.

[35] J.A. Zazo, J. Bedia, C.M. Fierro, G. Pliego, J.A. Casas, J.J. Rodriguez, Highly stable Fe on activated carbon catalysts for CWPO upon FeCl3 activation of lignin from black liquors, Catal. Today. 187 (2012) 115–121. doi:10.1016/j.cattod.2011.10.003.

[36] S. Brunauer, P.H. Emmett, E. Teller, Adsorption of Gases in Multimolecular Layers, J. Am. Chem. Soc. 60 (1938) 309–319. doi:10.1021/ja01269a023.

[37] B.C. Lippens, de B. J.H., Studies on pore systems in catalysts: V. The t method, J. Catal. 4 (1965) 319–323. doi:10.1016/0021-9517(65)90307-6.

[38] J. Tauc, Absorption edge and internal electric fields in amorphous semiconductors, Mater. Res. Bull. 5 (1970) 721–729. doi:10.1016/0025-5408(70)90112-1.

[39] J. Zhang, P. Zhou, J. Liu, J. Yu, New understanding of the difference of photocatalytic activity among anatase, rutile and brookite TiO2, Phys. Chem. Chem. Phys. 16 (2014) 20382–20386. doi:10.1039/c4cp02201g.

[40] G. Newcombe, R. Hayes, M. Drikas, Granular activated carbon: Importance of surface properties in the adsorption of naturally occurring organics, Colloids Surfaces A Physicochem. Eng. Asp. 78 (1993) 65–71. doi:10.1016/0927-7757(93)80311-2.

[41] F. Tian, Z. Wu, Q. Chen, Y. Yan, G. Cravotto, Z. Wu, Microwave-induced crystallization of AC/TiO_2 for improving the performance of rhodamine B dye degradation, Appl. Surf. Sci. 351 (2015) 104–112. doi:10.1016/j.apsusc.2015.05.133.

[42] D. Liu, Z. Wu, F. Tian, B.C. Ye, Y. Tong, Synthesis of N and La co-doped TiO_2/AC photocatalyst by microwave irradiation for the photocatalytic degradation

of naphthalene, J. Alloys Compd. 676 (2016) 489–498. doi:10.1016/j.jallcom.2016.03.124.

[43] S. Horikoshi, S. Sakamoto, N. Serpone, Formation and efficacy of TiO2/AC composites prepared under microwave irradiation in the photoinduced transformation of the 2-propanol VOC pollutant in air, Appl. Catal. B Environ. 140–141 (2013) 646–651. doi:10.1016/j.apcatb.2013.04.060.

[44] M. Thommes, K. Kaneko, A. V. Neimark, J.P. Olivier, F. Rodriguez-Reinoso, J. Rouquerol, K.S.W. Sing, Physisorption of gases, with special reference to the evaluation of surface area and pore size distribution (IUPAC Technical Report), Pure Appl. Chem. 87 (2015) 1051–1069. doi:10.1515/pac-2014-1117.

[45] A.C. Martins, A.L. Cazetta, O. Pezoti, J.R.B. Souza, T. Zhang, E.J. Pilau, T. Asefa, V.C. Almeida, Sol-gel synthesis of new TiO2/activated carbon photocatalyst and its application for degradation of tetracycline, Ceram. Int. 43 (2017) 4411–4418. doi:10.1016/j.ceramint.2016.12.088.

[46] R. Leary, A. Westwood, Carbonaceous nanomaterials for the enhancement of TiO_2 photocatalysis, Carbon N. Y. 49 (2011) 741–772. doi:10.1016/j.carbon.2010.10.010.

[47] N.R. Khalid, A. Majid, M.B. Tahir, N.A. Niaz, S. Khalid, Carbonaceous-TiO_2 nanomaterials for photocatalytic degradation of pollutants: A review, Ceram. Int. 43 (2017) 14552–14571. doi:10.1016/j.ceramint.2017.08.143.

[48] M. Akkari, P. Aranda, C. Belver, J. Bedia, A. Ben Haj Amara, E. Ruiz-Hitzky, ZnO/sepiolite heterostructured materials for solar photocatalytic degradation of pharmaceuticals in wastewater, Appl. Clay Sci. 156 (2018) 104–109. doi:10.1016/j.clay.2018.01.021.

[49] C. Belver, J. Bedia, J.J. Rodriguez, Zr-doped TiO2 supported on delaminated clay materials for solar photocatalytic treatment of emerging pollutants, J. Hazard. Mater. 322 (2017) 233–242. doi:10.1016/j.jhazmat.2016.02.028.

[50] A. Gómez-Avilés, M. Peñas-Garzón, J. Bedia, D.D. Dionysiou, J.J. Rodríguez, C. Belver, Mixed Ti-Zr metal-organic-frameworks for the photodegradation of acetaminophen under solar irradiation, Appl. Catal. B Environ. 253 (2019) 253–262. doi:10.1016/j.apcatb.2019.04.040.

[51] N. Jallouli, K. Elghniji, H. Trabelsi, M. Ksibi, Photocatalytic degradation of paracetamol on TiO2 nanoparticles and TiO2/cellulosic fiber under UV and sunlight irradiation, Arab. J. Chem. 10 (2017) S3640–S3645.

doi:10.1016/j.arabjc.2014.03.014.

[52] C. Belver, M. Hinojosa, J. Bedia, M. Tobajas, M.A. Alvarez, V. Rodríguez-González, J.J. Rodriguez, Ag-Coated heterostructures of ZnO-TiO2/delaminated montmorillonite as solar photocatalysts, Materials (Basel). 10 (2017) 960. doi:10.3390/ma10080960.

[53] A. Eslami, M.M. Amini, A.R. Yazdanbakhsh, A. Mohseni-Bandpei, A.A. Safari, A. Asadi, N,S co-doped TiO2 nanoparticles and nanosheets in simulated solar light for photocatalytic degradation of non-steroidal anti-inflammatory drugs in water: a comparative study, J. Chem. Technol. Biotechnol. 91 (2016) 2693–2704. doi:10.1002/jctb.4877.

[54] G. Di, Z. Zhu, H. Zhang, J. Zhu, H. Lu, W. Zhang, Y. Qiu, L. Zhu, S. Küppers, Simultaneous removal of several pharmaceuticals and arsenic on Zn-Fe mixed metal oxides: Combination of photocatalysis and adsorption, Chem. Eng. J. 328 (2017) 141–151. doi:10.1016/j.cej.2017.06.112.

[55] A.M. Amado, C. Azevedo, P.J.A. Ribeiro-Claro, Conformational and vibrational reassessment of solid paracetamol, Spectrochim. Acta Part A Mol. Biomol. Spectrosc. 183 (2017) 431–438. doi:10.1016/j.saa.2017.04.076.

[56] D.J. Goossens, A.P. Heerdegen, T.R. Welberry, A.G. Beasley, The molecular conformation of Ibuprofen, C13H18O2, through X-ray diffuse scattering, Int. J. Pharm. 343 (2007) 59–68. doi:10.1016/J.IJPHARM.2007.04.023.

[57] K.S. Venkatasubban, R. Rothchild, NMR Studies of Drugs: Antipyrine and Analogs. II. ^{1}H and ^{13}C Chemical Shift Dispersion as Conformation Indicator for the *N* -Phenyl Ring., Spectrosc. Lett. 30 (1997) 1685–1697. doi:10.1080/00387019708006752.

[58] M.M. Hinojosa Guerra, I. Oller Alberola, S. Malato Rodriguez, A. Agüera López, A. Acevedo Merino, A. Egea-Corbacho Lopera, J.M. Quiroga Alonso, Oxidation mechanisms of amoxicillin and paracetamol in the photo-Fenton solar process, Water Res. 156 (2019) 232–240. doi:10.1016/j.watres.2019.02.055.

[59] R. Andreozzi, V. Caprio, R. Marotta, D. Vogna, Paracetamol oxidation from aqueous solutions by means of ozonation and H2O2/UV system, Water Res. 37 (2003) 993–1004. doi:10.1016/S0043-1354(02)00460-8.

[60] S. Wang, J. Wu, X. Lu, W. Xu, Q. Gong, J. Ding, B. Dan, P. Xie, Removal of acetaminophen in the Fe2+/persulfate system: Kinetic model and degradation pathways, Chem. Eng. J. 358 (2019) 1091–1100. doi:10.1016/j.cej.2018.09.145.

[61] H. Lee, I.S. Park, H.J. Bang, Y.K. Park, H. Kim, H.H. Ha, B.J. Kim, S.C. Jung, Fabrication of Gd-La codoped TiO 2 composite via a liquid phase plasma method and its application as visible-light photocatalysts, Appl. Surf. Sci. 471 (2019) 893–899. doi:10.1016/j.apsusc.2018.11.249.

[62] C.T. Chang, J.J. Wang, T. Ouyang, Q. Zhang, Y.H. Jing, Photocatalytic degradation of acetaminophen in aqueous solutions by TiO2/ZSM-5 zeolite with low energy irradiation, Mater. Sci. Eng. B Solid-State Mater. Adv. Technol. 196 (2015) 53–60. doi:10.1016/j.mseb.2014.12.025.

[63] Y. Chen, X. Zhang, L. Mao, Z. Yang, Dependence of kinetics and pathway of acetaminophen photocatalytic degradation on irradiation photon energy and TiO2 crystalline, Chem. Eng. J. 330 (2017) 1091–1099. doi:10.1016/j.cej.2017.07.148.

[64] Y. Xiang, J. Fang, C. Shang, Kinetics and pathways of ibuprofen degradation by the UV/chlorine advanced oxidation process, Water Res. 90 (2016) 301–308. doi:10.1016/j.watres.2015.11.069.

[65] N. Liu, W. Huang, M. Tang, C. Yin, B. Gao, Z. Li, L. Tang, J. Lei, L. Cui, X. Zhang, In-situ fabrication of needle-shaped MIL-53(Fe) with 1T-MoS2 and study on its enhanced photocatalytic mechanism of ibuprofen, Chem. Eng. J. 359 (2019) 254–264. doi:10.1016/j.cej.2018.11.143.

[66] L. Lin, W. Jiang, M. Bechelany, M. Nasr, J. Jarvis, T. Schaub, R.R. Sapkota, P. Miele, H. Wang, P. Xu, Adsorption and photocatalytic oxidation of ibuprofen using nanocomposites of TiO2 nanofibers combined with BN nanosheets: Degradation products and mechanisms, Chemosphere. 220 (2019) 921–929. doi:10.1016/j.chemosphere.2018.12.184.

[67] M. Tanveer, G.T. Guyer, G. Abbas, Photocatalytic degradation of ibuprofen in water using TiO2 and ZnO under artificial UV and solar irradiation, Water Environ. Res. 91 (2019) 822–829. doi:10.1002/wer.1104.

[68] Z. dong Lei, J. jun Wang, L. Wang, X. yu Yang, G. Xu, L. Tang, Efficient photocatalytic degradation of ibuprofen in aqueous solution using novel visible-light responsive graphene quantum dot/AgVO3 nanoribbons, J. Hazard. Mater. 312 (2016) 298–306. doi:10.1016/j.jhazmat.2016.03.044.

[69] J.C.C. Da Silva, J.A.R. Teodoro, R.J. de C.F. Afonso, S.F. Aquino, R. Augusti, Photolysis and photocatalysis of ibuprofen in aqueous medium: Characterization of by-products via liquid chromatography coupled to high-resolution mass spectrometry and assessment of their toxicities against Artemia Salina, J. Mass

Spectrom. 49 (2014) 145–153. doi:10.1002/jms.3320.
[70] H.F. Miao, M. Cao, D.Y. Xu, H.Y. Ren, M.X. Zhao, Z.X. Huang, W.Q. Ruan, Degradation of phenazone in aqueous solution with ozone: Influencing factors and degradation pathways, Chemosphere. 119 (2015) 326–333. doi:10.1016/j.chemosphere.2014.06.082.
[71] H. Gong, W. Chu, M. Chen, Q. Wang, A systematic study on photocatalysis of antipyrine: Catalyst characterization, parameter optimization, reaction mechanism a toxicity evolution to plankton, Water Res. 112 (2017) 167–175. doi:10.1016/j.watres.2017.01.041.
[72] F. Yuan, C. Hu, X. Hu, J. Qu, M. Yang, Degradation of selected pharmaceuticals in aqueous solution with UV and UV/H2O2, Water Res. 43 (2009) 1766–1774. doi:10.1016/j.watres.2009.01.008.
[73] A.J. Expósito, D.A. Patterson, W.S.W. Mansor, J.M. Monteagudo, E. Emanuelsson, I. Sanmartín, A. Durán, Antipyrine removal by TiO2 photocatalysis based on spinning disc reactor technology, J. Environ. Manage. 187 (2017) 504–512. doi:10.1016/j.jenvman.2016.11.012.
[74] J.M. Monteagudo, A. Durán, J. Latorre, A.J. Expósito, Application of activated persulfate for removal of intermediates from antipyrine wastewater degradation refractory towards hydroxyl radical, J. Hazard. Mater. 306 (2016) 77–86. doi:10.1016/j.jhazmat.2015.12.001.

Degradation pathways of emerging contaminants using TiO_2-activated carbon heterostructures in aqueous solution under simulated solar light

M. Peñas-Garzón, A. Gómez-Avilés, C. Belver*, J.J. Rodriguez, J. Bedia

Chemical Engineering Department, Universidad Autónoma de Madrid, Campus Cantoblanco, E-28049 Madrid, Spain

*Corresponding author. E-mail address: carolina.belver@uam.es

Keywords: Activated carbon; TiO_2/carbon-heterostructures; solar photocatalysis; water treatment; pharmaceutical degradation pathways.

Abstract

This work deals with the degradation of three emerging contaminants (acetaminophen, ibuprofen and antipyrine) in water under simulated solar light using different catalysts of TiO_2/activated carbon heterostructures. The heterostructures, based on anatase phase, were successfully synthesized following three different methods (solvothermal, microwave-assisted and sol-gel), using lignin as carbon precursor. The sol-gel photocatalyst only yielded 50% conversion of acetaminophen and a low mineralization (15%), probably due to the higher crystal and particle sizes and lower surface area of this heterostructure, as a consequence of the higher temperature reached during the heat-treatment included in this synthesis route to achieve anatase crystallization. In contrast, the heterostructure prepared by the microwave-assisted procedure achieved complete conversion after 6 h of reaction. Regarding the contaminants, ibuprofen was the most easily removed, requiring 3 h for complete disappearance, while antipyrine showed the highest resistance to photodegradation, not being completely removed after 6 h. The photocatalytic performance was also evaluated for a mixture of these three pharmaceuticals at different initial pH. The fastest and highest mineralization (ca. 50 %) occurred around neutral pH. The study proposes the oxidation degradation pathways of the three pharmaceuticals under solar-simulated irradiation from the analysis of the reaction intermediates.

1. Introduction

The awareness about the presence of contaminants of emerging concern (CECs) in water bodies is strongly increasing, especially in the last two decades. This type of compounds, also known as emerging contaminants due to recent detection and quantification in water streams, are considered to be biologically active, altering the metabolism of living beings, despite they are usually detected in very low concentrations [1–5]. CECs include, among other species, pharmaceuticals and personal care products that are considered endocrine disruptors and can cause negative effects on health and aquatic environments due to their continuous release [6,7]. They are commonly present in sewage and wastewater treatment plants (WWTPs) allow only partial removal in most cases, so that continuous municipal discharges give rise to accumulation in the receiving water bodies. The average removal of antibiotics in WWTPs has been reported in the range of 40-60% and close to 25-55% in the case of analgesics and anti-inflammatories [8,9]. These species can be also present in the wastewaters from pharmaceutical plants, in this case at substantially higher concentrations, in the order of $mg \cdot L^{-1}$. The growing concern about water quality promotes action plans by United Nations [10] and research efforts on the development of efficient and sustainable technologies for the abatement of those pollutants, in general of hazardous character.

Several advanced treatments have been investigated for the removal of CECs [11,12], including advanced oxidation processes (AOPs), which degrade contaminants via generation of reactive oxygen species (ROS). Among the AOPs, heterogeneous photocatalysis has been widely reported for the removal of many different types of contaminants [13]. In this technology, ROS can be generated upon light absorption in a semiconductor (being TiO_2 the most used so far) giving rise to separation of electron-hole charges. Nowadays, there is a growing trend to use solar light as renewable and sustainable energy source, reducing the operation costs [8]. In spite of the wide use of TiO_2 (due to its well-stated physical and chemical properties), this material has the main drawbacks of low adsorption capacity, limited photocatalytic activity under visible light and difficult recovery from the aqueous medium, especially in the case of commercial TiO_2 [14]. Supporting TiO_2 on porous materials, as activated carbons (ACs), zeolites or clays, can partly overcome these drawbacks [15,16]. ACs are characterized by their relatively low cost, high surface area and well-developed porosity. Moreover, activated carbons can be prepared from almost any carbonaceous waste, providing a way of

valorization of those residues. Lignin, a biopolymer with relatively high carbon content is a main component of lignocellulosic biomass. Different types of modified lignin are produced in huge amounts from cellulose pulp manufacture, being mostly used by its fuel value. The future development of biorefinery is expected to generate high quantities of waste lignin whose valorization becomes mandatory. Regarding valorization possibilities, lignin has been studied as precursor for the synthesis of activated carbons and other carbon-based materials [17–26]. In a recent work [27], our research group investigated the use of different activating agents ($FeCl_3$, $ZnCl_2$, H_3PO_4 and KOH) in the preparation of activated carbons from lignin for synthesizing TiO_2/activated carbon heterostructures. It was observed that the photocatalyst obtained with $FeCl_3$-activated carbon yielded higher removal of acetaminophen (around 29, 42 and 74% higher than those obtained with KOH-, H_3PO_4- and $ZnCl_2$-derived carbons, respectively, after 3 h under solar light). In that previous research, the photocatalytic performance of bare TiO_2 was already studied, being higher than the synthesized TiO_2/AC heterostructures, which was attributed to a better contact of contaminant with non-supported TiO_2 as corroborated in literature [28]. However, the photocatalyst obtained with $FeCl_3$-activated carbon showed around 5-fold increment in the initial settling velocity compared to bare TiO_2, and therefore it is much easily recovered from the reaction media.

The preparation of the TiO_2/AC heterostructures can be addressed by different methods [29–32]. The properties of these heterostructures depend on the synthesis route because of the different conditions used. For instance, sol-gel synthesis requires high temperature post-treatment to obtain the highly-photoactive anatase phase; solvothermal synthesis uses lower temperatures, while microwave-assisted methodology allows a faster heating rate and different distribution of heat involving hot spots [28]. To the best of our knowledge, a detailed comparative study of the performance of TiO_2-carbonaceous heterostructures prepared by these three synthesis routes on the photocatalytic degradation of emerging contaminants has not been reported before. Additionally, in many cases it has not been established a clear difference between the contribution of adsorption and photodegradation, despite this can be a key factor when using highly porous materials as catalyst supports. In the current study, TiO_2/AC heterostructures have been synthesized by three different methods (solvothermal, microwave-assisted and sol-gel), being the activated carbon previously prepared by chemical activation of lignin with $FeCl_3$. The synthesized heterostructures have been tested in the solar-driven photocatalytic

degradation of three target pharmaceuticals (acetaminophen, ibuprofen and antipyrine), paying special attention to the effect of pH and the extent of mineralization. Experiments with three single compounds as well as with mixtures of them have been performed. In addition to this, intermediates of the photocatalytic oxidation of individual contaminants were identified, being proposed the degradation pathways of these pharmaceuticals under solar-simulated light.

2. Materials and Methods

2.1. Materials

The activated carbon used was synthesized from lignin (supplied by LignoTech Iberica S.A.) as carbon source and $FeCl_3 \cdot 6H_2O$ (≥97%, Panreac) as activating agent. Ethanol (EtOH; 96%, Panreac) was used as solvent in the synthesis of the heterostructures. Titanium tetrabutoxide ($Ti(OBu)_4$; ≥97%) and titanium isopropoxide ($Ti(OiPr)_4$; ≥97%) were used as titania precursors and both were supplied by Sigma Aldrich. The photocatalytic performance was tested in the degradation of acetaminophen (ACE; ≥99%), ibuprofen (IBU; ≥98%) and antipyrine (ANT; ≥99%), all purchased from Sigma Aldrich (their chemical structures can be seen in Figure S1 of the Supplementary Information). NaOH (≥95%) and HCl (≥37%) were used as pH-modifiers and purchased from Scharlau and Sigma Aldrich, respectively. NaCl (>99.5%) was supplied by Panreac. The mobile phase for liquid chromatography consisted of acetic acid (≥99%, Sigma Aldrich) and acetonitrile (ACN, HPLC grade, Scharlau). Finally, ultrapure water (Type I, 18.2 MΩ·cm) and deionized water (Type II) were used throughout the work.

2.2. Preparation of activated carbon (AC)

Following our previous results on the synthesis of TiO_2/AC heterostructures [27], we selected $FeCl_3$ as activating agent to prepare the lignin-derived AC [33–35]. Lignin and $FeCl_3$ (1:3 mass ratio) were physically mixed and dried at 60 ºC overnight. Then, the mixture was heat-treated using a horizontal stainless-steel tubular furnace at 800 ºC (heating rate of 10 ºC·min^{-1}) for 2 h under inert atmosphere (N_2, 150 cm^3 STP·min^{-1}). After cooling, the resulting material was firstly washed with 0.1 M HCl at 70 ºC for 2 h to remove the residual activating agent and free the porosity. Then, it was rinsed to neutral pH using ultrapure water at room temperature. The activated carbon was finally dried at 60 ºC overnight, stored and labelled as AC.

2.3. Synthesis of TiO_2/AC heterostructures

Three different routes were followed to prepare the TiO_2/AC heterostructures. In all cases, a TiO_2:AC mass ratio of 4:1 was used [27]. Other TiO_2:AC mass ratios were also tested, but 4:1 led to the best photocatalysts. The amount of water was stoichiometrically fixed to promote the hydrolysis and condensation of the titania precursor.

2.3.1. Solvothermal (ST) route.

The solvothermal synthesis of the TiO_2/AC heterostructure has been described elsewhere [27]. Briefly, a suspension (A1) of 58 mg of AC in 45 mL of EtOH was firstly prepared at room temperature. Then, a solution (B1), obtained by diluting 1 mL of $Ti(OBu)_4$ in 15 mL of EtOH, was added to A1 under continuous stirring. Subsequently, 3 mL of ultrapure water were added to 15 mL of EtOH (solution C1) dropwise to hydrolyze the $Ti(OBu)_4$. Finally, the mixture was stirred for 5 min, placed in a 125 mL Teflon-lined stainless-steel autoclave and heated at 160 ºC for 3 h in an oven (Memmert UN30). The resulting solid was separated by centrifugation (5300 rpm, 10 min) and washed once with EtOH and four times with ultrapure water. The sample was finally dried at 60 ºC overnight and labelled as TiO_2/AC-ST.

2.3.2. Microwave-assisted (MW) route.

The microwave-assisted route was based on the method described by Orha et al. [32]. In this synthesis, 37.1 mg of AC were suspended in 28.5 mL of EtOH (solution A2). Other two solutions were prepared by diluting 0.633 mL of $Ti(OBu)_4$ in 9.5 mL of EtOH (solution B2); and 1.9 mL ultrapure water into 9.5 mL of EtOH (solution C2). Then, A2 and B2 were mixed under continuous stirring, while C2 was further dropwise incorporated. The final mixture was transferred to a 100 mL Teflon-lined reactor and then inserted in a SK-15 Microwave Digestion Rotor (Milestone). The synthesis was performed setting 175 ºC as constant temperature (600 W as maximum microwave power input) for 30 min. The resulting solid was separated by centrifugation, washed and dried as described for the previous solvothermal route. The resulting material was named as TiO_2/AC-MW.

2.3.3. Sol-gel (SG) route.

The sol-gel synthesis of TiO_2/AC heterostructure was slightly modified from a previous work of Belver et al. [16]. In this method, a suspension of 67.2 mg of AC in 12.5 mL of

EtOH was firstly prepared (solution A3); then, 1 mL of $Ti(OiPr)_4$ was added to 1.9 mL of EtOH (solution B3). Meanwhile, solution C3 was prepared adding 0.25 mL of ultrapure water to 1.75 mL of EtOH. A3 and B3 were mixed under stirring in a 100 mL glass beaker while C3 was slowly added favoring homogenous dispersion. The beaker was sealed with parafilm and the mixture was then heated at 50 ºC during 72 h, under stirring. During this time, a dense gel was obtained after the spontaneous coagulation of the mixture. Thereafter, the gel was dried at room temperature for 72 h. The resulting solid was heat-treated at 500 ºC for 2 h under inert atmosphere (N_2, 150 cm^3 $STP \cdot min^{-1}$) inside a horizontal stainless-steel tubular furnace. The resulting heterostructure was labelled as TiO_2/AC-SG. In this synthesis, $Ti(OiPr)_4$ was selected as titania precursor due to the faster hydrolyzation of $Ti(OBu)_4$ in contact with water, which gives rise to the formation of high-size agglomerates of titanium oxyhydroxides. This precursor makes difficult obtaining anatase phase with low crystal size. $Ti(OiPr)_4$, whose hydrolysis rate is lower, allowing to obtain the desired anatase with low crystal size.

2.4. Characterization of the photocatalysts.

Elemental analysis was carried out in a LECO CHNS-932 to determine the content of carbon (C) in the synthesized samples. The quantification of TiO_2 in the different heterostructures was accomplished by wavelength-dispersive X-ray fluorescence (WDXRF) using a Bruker S8 TIGER spectrometer under inert atmosphere (He) with a maximum voltage of 60 kV and a maximum current of 170 mA. Spectra Plus (v. 3) software was used to determine the composition of the materials. A Bruker D8 diffractometer was used to obtain the X-ray diffraction (XRD) patterns, using Cu-Kα (λ = 0.154 nm) source (2θ range from 5 to 70º, scan step of $5^{o} \cdot min^{-1}$). The most intense diffraction peak (101) of anatase phase was used to estimate the average crystal size (D) using the Scherrer's equation. The morphology of the heterostructures was observed by scanning electron microscopy (SEM) using a Quanta 3D Field Emission Gun (FEG) microscope (FEI Company). The distribution of TiO_2 particle size was obtained from SEM micrographs using ImageJ software, taking several images to obtain a representative result. A Micromeritics TriStar 123 static volumetric system was used to obtain the N_2 adsorption-desorption isotherms at −196 ºC after outgassing the samples under vacuum at 150 ºC overnight in a Florprep 060 Micromeritics equipment. The Brunauer-Emmett-Teller (BET) method [36] was used to obtain the specific surface area (S_{BET}), whereas both microporous (S_{MP}) and non-microporous surface area (S_{EXT}) were calculated by the t-

plot method [37]. Total pore volume (V_T) was estimated by the amount of nitrogen adsorbed at a relative pressure (P/P_0) of 0.99. UV-vis diffuse reflectance spectra (UV-vis DRS) were recorded in a Shimadzu 2501PC UV–vis spectrophotometer in the 250–800 nm wavelength range using $BaSO_4$ as reference material. The band gap (E_g) values of the heterostructures were obtained from the UV-vis DRS spectra, through the Tauc Plot method [38], considering the synthesized photocatalysts as indirect semiconductors [39]. The pH at the point of zero charge (pH_{pzc}) was determined by the pH drift method [27,40]. The photoluminescence (PL) spectra of the powder samples were obtained in a Perkin Elmer LS50B spectrofluorometer using an excitation wavelength of 275 nm and a sample holder with a quartz window.

2.5. Photocatalytic performance

The photocatalytic activity of the different heterostructures was evaluated for the degradation of acetaminophen (ACE), ibuprofen (IBU) and antipyrine (ANT) under solar-simulated irradiation. A 500 mL Pyrex closed jacketed reactor was placed inside a Suntest XLS+ (Atlas), under continuous stirring and controlled temperature (25 ºC) with a refrigerated/heating circulator 200F (Julabo). The irradiation intensity, provided by a Xe lamp (765–250 $W \cdot m^{-2}$) with a "Daylight" filter (restrains $\lambda \leq 290$ nm), was fixed at 600 $W \cdot m^{-2}$ (107.14 klx). In a typical experiment, the concentration of the photocatalyst was adjusted to 250 $mg \cdot L^{-1}$ of TiO_2, considering to the composition of the heterostructures as obtained by WDXRF. Thereafter, the photocatalyst was dispersed in a deionized water solution (150 mL) of the selected contaminant at natural pH, being 6.78, 7.05 and 7.08 for ACE, IBU and ANT, respectively. Prior to these experiments, it was observed that each heterostructure showed different adsorption capacity. Consequently, each photocatalyst was dispersed in solutions with different initial concentrations of each contaminant, in order to adjust the concentration of each contaminant at 5 $mg \cdot L^{-1}$ before starting the irradiation (after adsorption equilibrium). Finally, the photocatalytic experiments were carried out for 6 h under simulated solar light. The experiments were all performed by triplicate and the 95% confidence interval was included. Specific experiments were carried out with a mixture of the three pharmaceuticals, setting the initial concentration of each compound to 5 $mg \cdot L^{-1}$ and adjusting the pH values from 3 to 11 with diluted HCl or NaOH.

At different irradiation times, samples of 450 μL were extracted from the reaction medium and filtered using Whatman 0.2 μm PTFE syringeless filters (Scharlau). A Shimadzu Prominence-I LC-2030C (diode array detector (SPD-M30A)), was used to analyze the aliquots of the reaction by High Performance Liquid Chromatography (HPLC), using a reverse phase C18 column. A mixture of acetonitrile/acetic acid 0.1% v/v was used as mobile phase (0.7 $mL \cdot min^{-1}$). A gradient method 10/90–40/60% was used for the quantification of ACE and ANT (detection λ = 246 and 242 nm, respectively), while IBU was determined by an isocratic 50/50% method (λ = 270 nm). On the other hand, a Shimadzu TOC-L analyzer was used to measure the total organic carbon (TOC) at the beginning (TOC_0) and end (TOC_f) of each photocatalytic test. Thus, the mineralization of the contaminants was followed by the TOC removal (%). The intermediate products from the pharmaceuticals tested were identified by Liquid Chromatography followed by Electrospray Ionization-Mass spectrometry (LC/ESI-MS). A Bruker Maxis II system with electrospray ionization (ESI) was used in positive ionization mode to follow the intermediates of ACE and ANT, whereas negative ionization mode was used for IBU (due to the presence of the carboxylic acid group). The analyses were performed with a capillary voltage of 3,500 V and an end plate offset of 500 V, at 300 ºC and 8 $mL \cdot min^{-1}$ of dry gas flow. Experimental data were collected in the range from 50 to 3,000 m/z with a full scan analysis of 0.1 s and a collision energy of 30 eV. Short-chain carboxylic acids and inorganic ions ~~they~~ were detected and quantified by ionic chromatography (IC), using a Metrohm 790 IC chromatograph with a Metrosep A Supp 5 (250 mm x 4 mm) column (Metrohm). As anionic eluent was used a 0.7 $mL \cdot min^{-1}$ aqueous solution of $Na_2CO_3/NaHCO_3$ (3.2 mM/1.0 mM) and H_2SO_4 (100.0 mM) as anionic suppressor.

3. Results and Discussion

3.1. TiO_2/AC heterostructures characterization

Table 1 summarizes the TiO_2 and C contents of the different heterostructures, whose values are quite similar to the nominally expected (TiO_2:AC mass ratio of 4:1) regardless of the synthetic route used. The three samples showed the characteristic peaks of the TiO_2 anatase phase (JCPDS 78-2486), as can be observed in the diffraction patterns depicted in Figure 1. It is important to remark that neither solvothermal (TiO_2/AC-ST) nor microwave-assisted (TiO_2/AC-MW) synthesis require of an additional high-temperature

heating step to obtain the anatase phase of titania. No other TiO_2 crystalline phases (rutile or brookite) were observed in any of the heterostructures. This result contrasts with previous studies on microwave-assisted synthesis of TiO_2 on activated carbons [41,42] that yielded titania in both anatase and rutile phases. The development of anatase as the only crystalline phase can be attributed to the fact that the synthesis route used in the current work was temperature-controlled, in contrast with those other studies where power-controlled approaches were used, implying higher temperatures and further crystallization into rutile. The average crystal size (D, Table 1) was calculated from the Scherrer's equation applied to the most intense peak of anatase (101). The crystal size of TiO_2 in the sol-gel sample (TiO_2/AC-SG) was more than two-fold the obtained for solvothermal and microwave-assisted heterostructures, which can be ascribed to the heat-treatment step at 500 ºC required to transform the titanium oxyhydroxide of the dried gel into titania. The TiO_2 crystal size in TiO_2/AC-ST and TiO_2/AC-MW (c.a. 10 nm) are similar to those previously reported for other supported titania photocatalysts from hydrothermal and microwave-assisted synthesis [30,32].

Table 1. Carbon and TiO_2 content, average crystal size (D) and band gap values (E_g) of the heterostructures.

Heterostructure	%C	%TiO_2[a]	D (nm)[b]	E_g (eV)
TiO_2/AC-ST	20.1	75.9	10.1	3.38
TiO_2/AC-MW	18.6	78.6	9.0	3.35
TiO_2/AC-SG	17.9	77.2	24.4	3.28

[a] Obtained by WDXRF. [b] From (101) anatase diffraction peak.

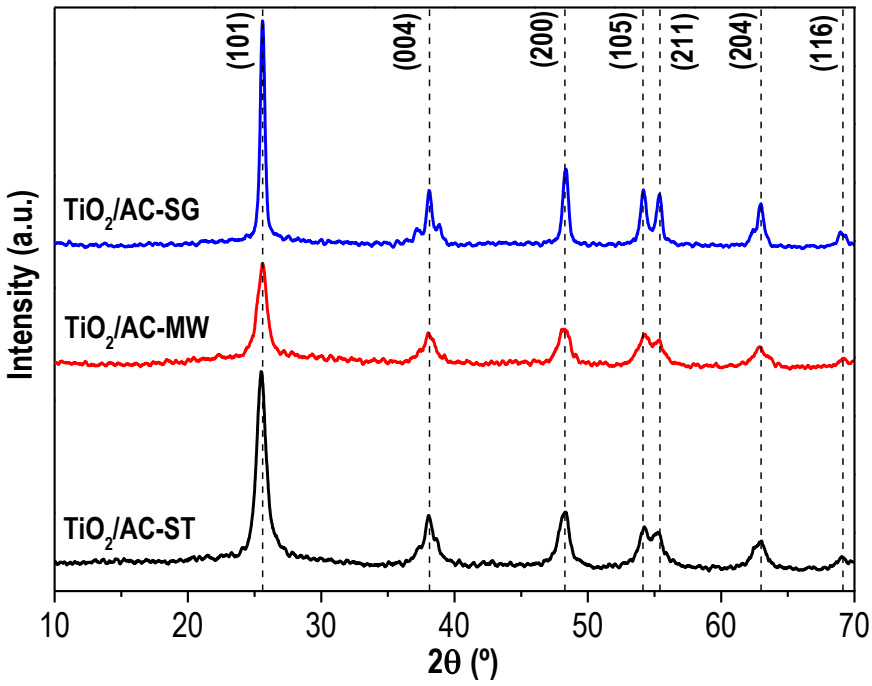

Figure 1. XRD patterns of the TiO_2/AC heterostructures. The characteristic diffraction peaks of anatase phase (JCPDS 78–2486) have been included.

Low-magnification SEM-images (Figure S2, Supplementary Information) revealed that the synthesized photocatalysts consisted of spherical TiO_2 nanoparticles distributed on the activated carbon surface. Figure 2 shows higher-magnification SEM micrographs and TiO_2 particle size distributions for the different heterostructures. The mean size of the TiO_2 particles decreased following the order: TiO_2/AC-SG (0.32 μm) > TiO_2/AC-MW (0.27 μm) > TiO_2/AC-ST (0.24 μm). Besides the highest TiO_2 particle size, TiO_2/AC-SG showed a broader distribution and much more uniform surface than the other heterostructures. These features can be ascribed to the aforementioned heat-treatment step, which removes the organic matter of the titanium precursor and caused its dehydroxylation, resulting in particle sinterization with a smoother surface. The TiO_2 mean particle size obtained in this work by microwave-assisted route is quite similar to those reported by Horikoshi et al. [43], who synthesized TiO_2 particles of ca. 0.25 μm at 180 ºC. Nevertheless, the TiO_2 particle size of TiO_2/AC-ST is higher than the reported by Liu et al. [30] for other TiO_2/commercial AC heterostructure prepared by hydrothermal synthesis.

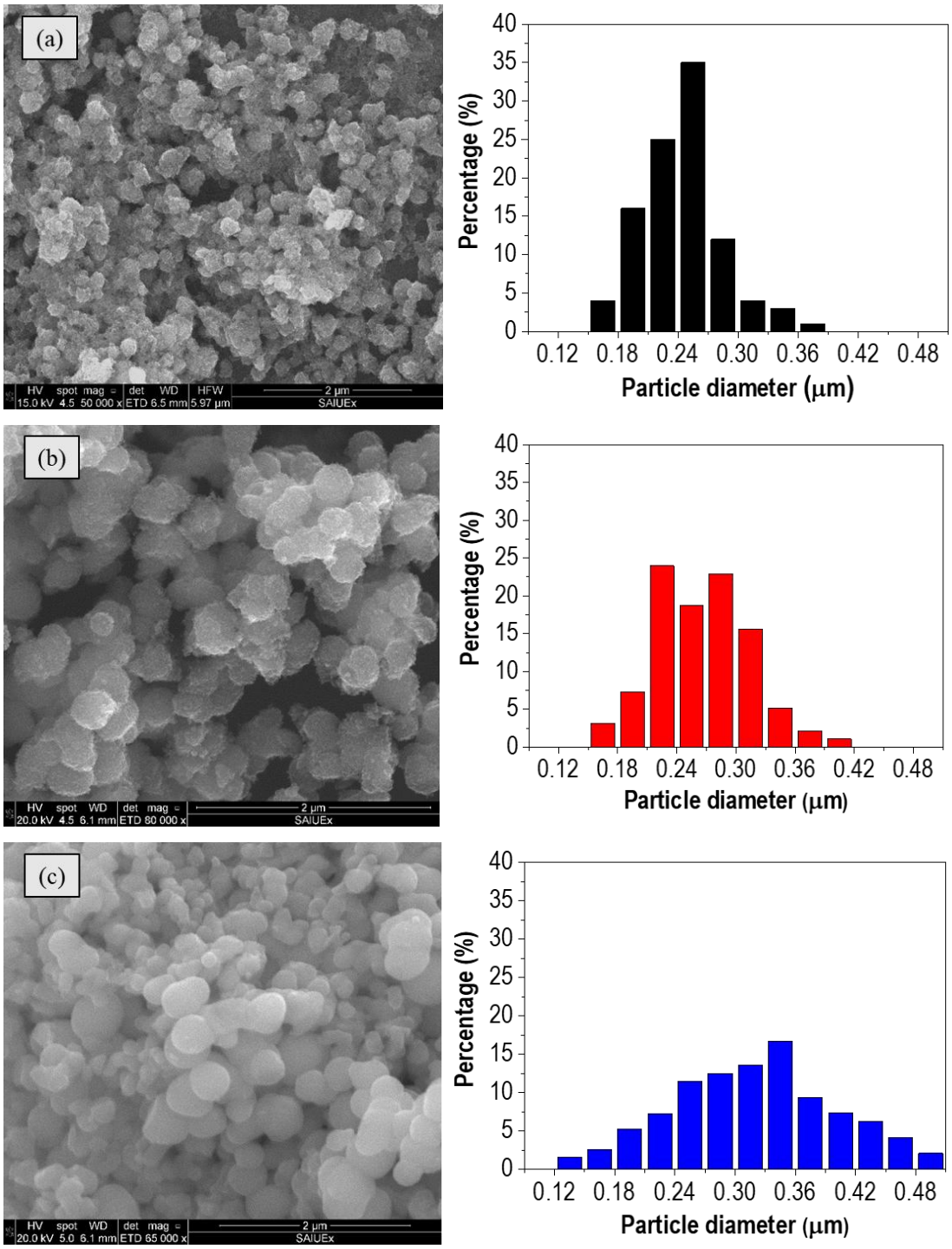

Figure 2. SEM micrographs and TiO_2 particle size distributions of the heterostructures: (a) TiO_2/AC-ST, (b) TiO_2/AC-MW and (c) TiO_2/AC-SG.

Figure 3 shows the -196 ºC N_2 adsorption-desorption isotherms of the activated carbon used as support and the three heterostructures synthesized. Meanwhile, Table 2 summarizes the porous textural characteristics derived from those isotherms. The AC showed a predominantly microporous texture with some minor contribution of

mesoporosity. This porous texture is comparable to the previously obtained from $FeCl_3$ activation of Tara gum [33] or sewage sludge [34]. On the other hand, both TiO_2/AC-ST and TiO_2/AC-MW exhibit type IV isotherms [44], characteristic of porous materials with contribution of both micro- and mesoporosity. It must be recalled that these heterostructures consist of almost 80% of TiO_2 and around 20% of AC. Thus, most of their porous texture is related to the porosity of the TiO_2 component and therefore controlled by the conditions for synthesizing the TiO_2 phase. The higher S_{EXT} values of TiO_2/AC-MW and TiO_2/AC-ST are a consequence of the higher amount of mesopores of these photocatalysts, as indicates the slope of their N_2 adsorption isotherms in the medium to high relative pressure range. Meanwhile, the TiO_2/AC-SG heterostructure showed a type I isotherm, indicative of a microporous solid. Its much lower porosity and surface area than the two other heterostructures, in spite of the quite similar TiO_2 and C contents, can be due to the heat treatment used for the crystallization of TiO_2. Martins et al. [45] reported quite similar values for a sol-gel synthesized TiO_2/activated carbon materials.

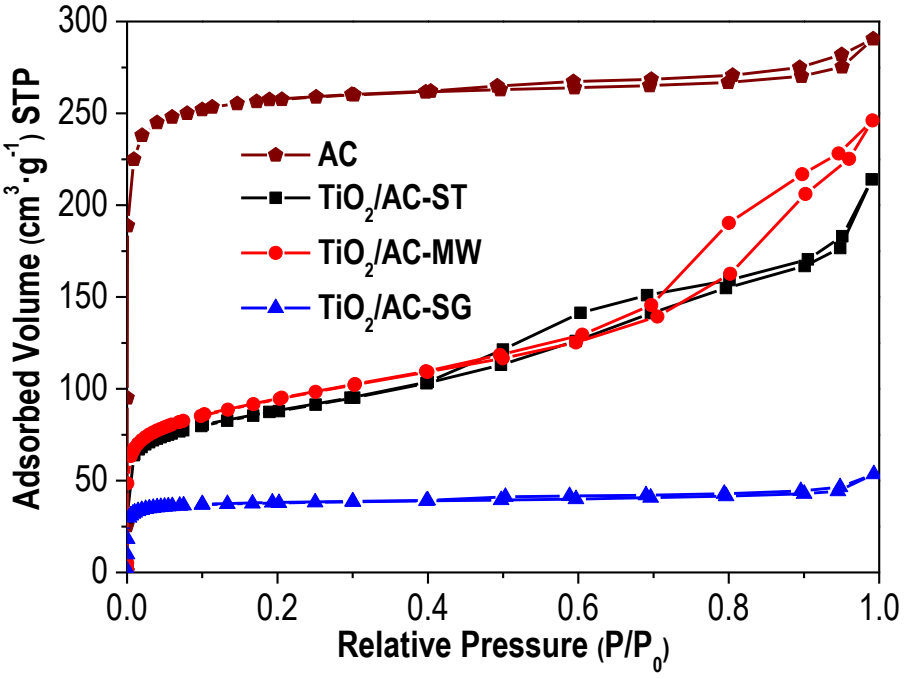

Figure 3. -196 ºC N_2 adsorption-desorption isotherms of the activated carbon (AC) and the TiO_2/AC heterostructures.

Table 2. Characterization of the porous texture of the AC and the heterostructures.

Sample	S_{BET} ($m^2 \cdot g^{-1}$)	S_{MP} ($m^2 \cdot g^{-1}$)	S_{EXT} ($m^2 \cdot g^{-1}$)	V_T ($cm^3 \cdot g^{-1}$)	V_{MP} ($cm^3 \cdot g^{-1}$)
AC	756	738	18	0.45	0.39
TiO_2/AC-ST	300	110	190	0.33	0.05
TiO_2/AC-MW	323	151	172	0.38	0.07
TiO_2/AC-SG	130	115	15	0.08	0.05

S_{BET}, specific surface area; S_{MP} and S_{EXT}, microporous and non-microporous surface area; V_T and V_{MP}, total and micropore volume.

The UV-Vis DRS absorption spectra of the photocatalysts are depicted in Figure 4a. The samples show the absorption band in the UV region ($\lambda < 400$ nm) corresponding to TiO_2 and also absorb a significant amount of radiation in the visible range, due to the presence of the activated carbon support, which confers to the samples their characteristic grey color. The estimated band gaps values (E_g) were obtained from the Tauc plots (Figure 4b), considering the heterostructures as indirect semiconductors (like the bare TiO_2). Since TiO_2 is supported on a carbon material that absorbs light because of its dark color, the band gaps were estimated from the extrapolation of the linear region to the background line of the support. The respective values are included in Table 1. All the heterostructures exhibit quite similar E_g values, close to that of bare TiO_2 [27,46,47], indicating that the interaction with the AC does not modify the TiO_2 band gap in any case.

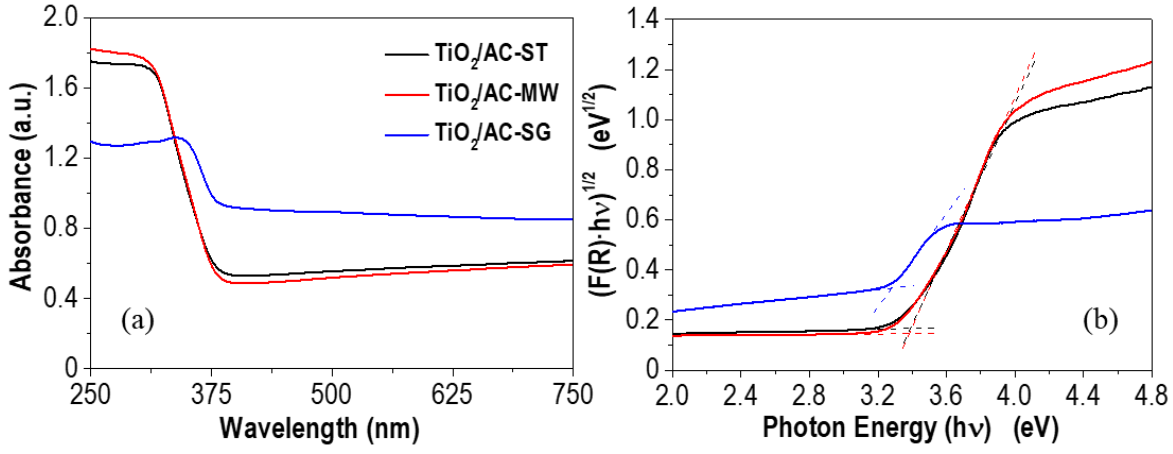

Figure 4. (a) UV–vis diffuse absorbance spectra and (b) Tauc plots of the TiO_2/AC heterostructures.

3.2. Photocatalytic performance

The different porosity and surface chemistry of the heterostructures can determine differences in the adsorption capacity. Then, prior to the photocatalytic tests, adsorption experiments with each target pollutant were carried out in dark for 16 h. This long-term stage (which can be illustrated by the pseudo second order kinetics of pharmaceutical adsorption onto the TiO_2/AC-MW heterostructure, see Table S1 and Figure S3) was performed to ensure the adsorption equilibrium of the contaminants, leading a better comparison of the photocatalytic performances. Taking into account adsorption results, the initial pollutant concentration was adjusted in order to have a liquid-phase concentration close to 5 $mg \cdot L^{-1}$ before irradiation. Thus, all the photocatalytic degradation tests were performed at almost similar starting concentrations of emerging contaminant. Figure 5 shows the evolution of ACE concentration upon irradiation time with all the TiO_2/AC heterostructures tested. A blank experiment in absence of photocatalyst was also performed, confirming that photolysis of ACE was almost negligible. TiO_2/AC-ST and TiO_2/AC-MW yielded a very similar disappearance rate of ACE, achieving almost complete conversion after 4 h under solar light, while TiO_2/AC-SG required 6 h to reach only ca. 50%. TOC removal after 6 h of reaction has been also included in Figure 5 (inset Table). TiO_2/AC-MW allowed the highest mineralization, 47%, somewhat higher than the achieved with TiO_2/AC-ST, while TiO_2/AC-SG yielded only 15% mineralization. This much poorer results with TiO_2/AC-SG can be initially associated to its higher crystal and particle size and lower porosity. Nevertheless, photocatalytic performance also depends on the transfer and recombination of the photogenerated charges. Thus, photoluminescence (PL) studies have been carried out considering that a reduction of the fluorescence intensity indicates a lower charge recombination rate. The resulting PL spectra are depicted in Figure 6. As can be seen, there are no major differences among the three heterostructures, just mention that the TiO_2/AC-MW spectrum has a slightly low intensity than that described by TiO_2/AC-ST. But the difference is very small, suggesting that the photoactivity is fundamentally controlled by the structural and textural properties. The results so far show that the sol-gel route, although it is conventionally used for the synthesis of TiO_2 heterostructures, does not seem to be the most appropriate looking at the photocatalytic performance of the resulting material. The microwave-assisted route appears as the best synthesis way in that respect.

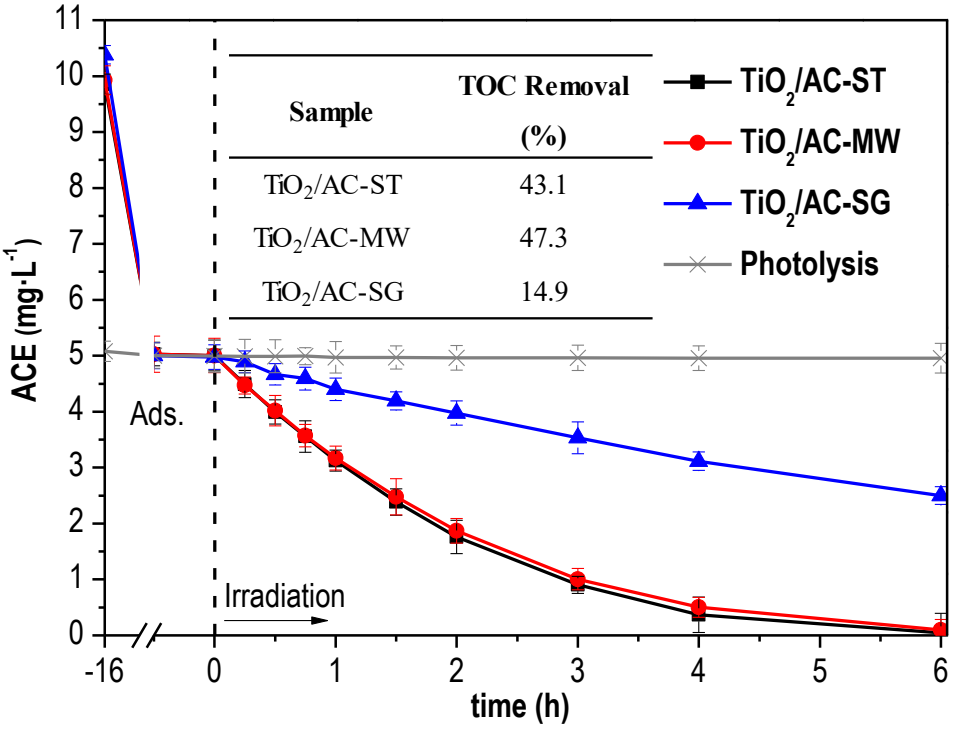

Figure 5. Time course of ACE concentration under solar irradiation with the heterostructures tested ([Photocatalyst]$_0$: 250 mg·L^{-1} of TiO_2; Intensity of irradiation: 600 W·m^{-2}).

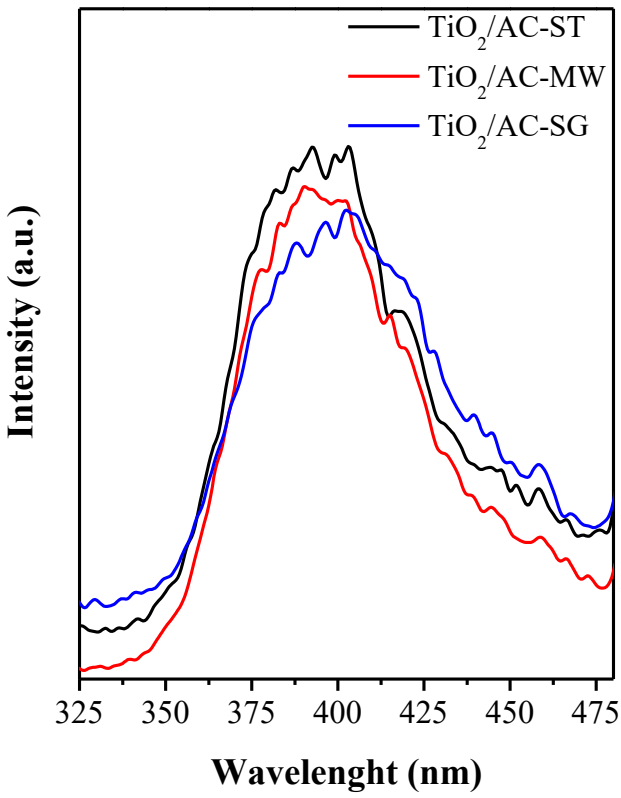

Figure 6. Photoluminescence spectra (PL) of the TiO_2/AC heterostructures.

Table 3 summarizes the values of the pseudo-first order rate constant of ACE disappearance with these materials and other heterostructures reported in previous works, all of them under solar light. The highest values obtained in the current study (ca. 0.50 h^{-1}) were significantly higher than the reported for ZnO/sepiolite [48], although somewhat lower than the corresponding to other TiO_2–based photocatalysts [49–52].

Table 3. Values of the first order kinetic constant, (h^{-1}), of ACE disappearance under solar light with this and other work materials.

Photocatalyst		Reference
TiO_2/AC-ST	0.50	This work
TiO_2/AC-MW	0.47	This work
TiO_2/AC-SG	0.11	This work
ZnO/sepiolite	0.19	[48]
Zr-doped TiO_2/clay	0.59	[49]
TiO_2(P25)/cellulosic fibers	0.61	[51]
Ag/ZnO-TiO_2/clay	0.57	[52]

Figure 7 depicts the evolution of IBU and ANT concentration upon photocatalytic degradation with TiO_2/AC-ST and TiO_2/AC-MW under solar irradiation (TiO_2/AC-SG was discarded due to its significantly lower photocatalytic performance). Both heterostructures allowed almost complete IBU conversion in less than 3 h, while that was not achieved for ANT even after 6 h. TiO_2/AC-MW exhibited somewhat higher photocatalytic activity with both pharmaceuticals. The inset Tables show the higher mineralization achieved with this last catalyst, being the difference significantly more pronounced for the degradation of ANT. Table 4 collects the values of the corresponding first order disappearance rate constant. Values previously reported with other photocatalysts have been also included for the sake of comparison. In the case of IBU the two heterostructures of the current work provided significantly faster degradation but the opposite was observed with ANT. It is noteworthy that the photocatalytic activity of ~~the~~ TiO_2/AC-MW depends on the nature of the target compound used. Comparing the results of Figures 5 and 7, and Tables 3 and 4, it appears that IBU is more easily degraded than ACE and the latter more than ANT. Considering the chemical structure of these pharmaceuticals (included in Figure S1 at Supplementary Information), it appears that

nitrogenous compounds are more refractory, being much more evident for ANT due to its pyrazolone group.

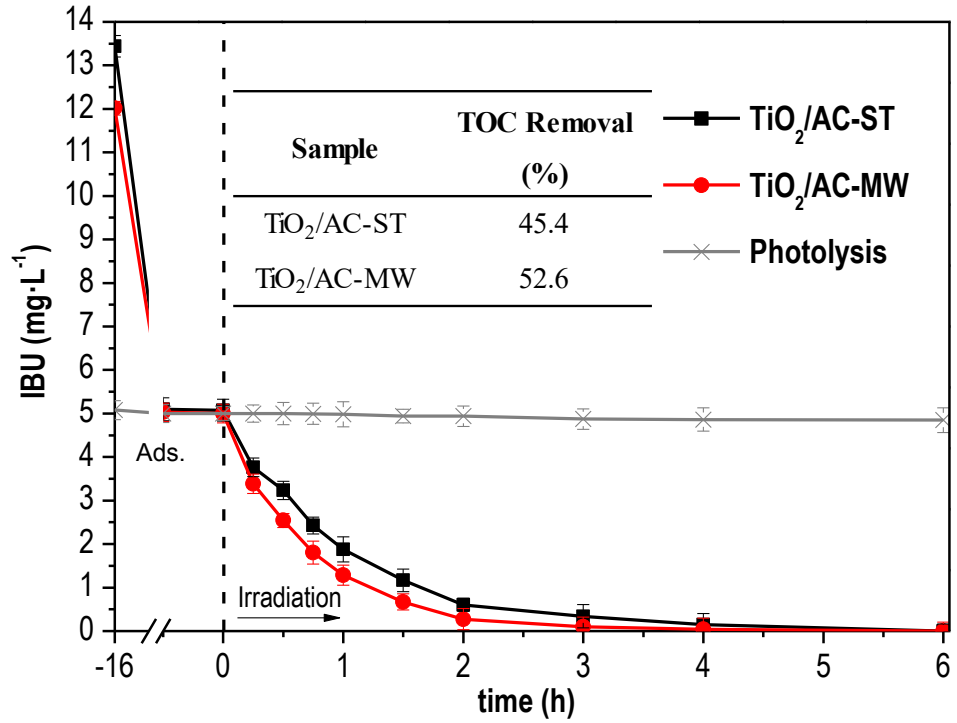

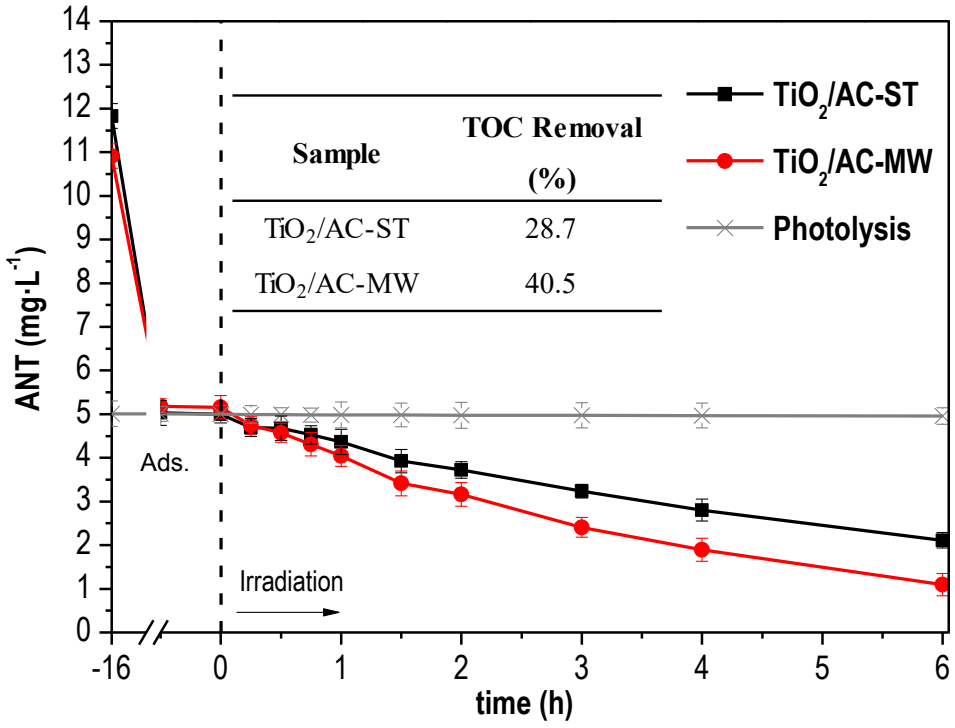

Figure 7. Time-course of IBU and ANT concentration upon solar photocatalytic degradation with the heterostructures tested. Operating conditions as in Figure 5.

Table 4. Values of the first order rate constant, (h^{-1}), of IBU and ANT disappearance under solar light with this and other works photocatalysts.

Photocatalyst	IBU	ANT	Reference
TiO_2/AC-ST	1.10	0.15	This work
TiO_2/AC-MW	1.40	0.25	This work
ZnO/sepiolite	0.38	0.13	[48]
Zr-doped TiO_2/clay	n.d.	0.58	[49]
Ag/ZnO-TiO_2/clay	n.d.	0.55	[52]
TiO_2	0.60	n.d.	[53]
ZnFe-MMOs	0.95	n.d.	[54]

n.d.: no data.

The TiO_2/AC-MW catalyst, the one giving the best results with each individual target compound was tested with a mixture of them. In this case, the initial concentration of each species was fixed at the same value of 5 $mg \cdot L^{-1}$ before the dark-adsorption step and so, different concentrations were remaining in solution at the start of solar irradiation, i.e., the photocatalytic stage. Figure 8 shows the results of this experiment. Firstly, very significant differences can be seen regarding the amount adsorbed of each target compound prior to the reaction, following the order ACE>>ANT>IBU. This order does not correspond with the expected from the previously observed in the single-compound experiments. Thus, competitive adsorption has a dramatic effect on the uptake of the individual species. Regarding photocatalytic conversion, the rate of disappearance is quite similar to the observed in the respective individual experiments, according to the values of the first-order rate constant (see Tables 3-5). Close to 50% mineralization was achieved after 6 h. An additional test was carried out using longer times, up to 24 h (Figure S4 of Supplementary Information), but, although almost complete conversion of the three target compounds was achieved, the TOC reduction remained almost unchanged, close to 50%, indicating the existence of degradation byproducts refractory to this treatment. In fact, it must also be considered that some byproducts can be adsorbed on the catalyst surface, which would lead a decrease of the mineralization rate.

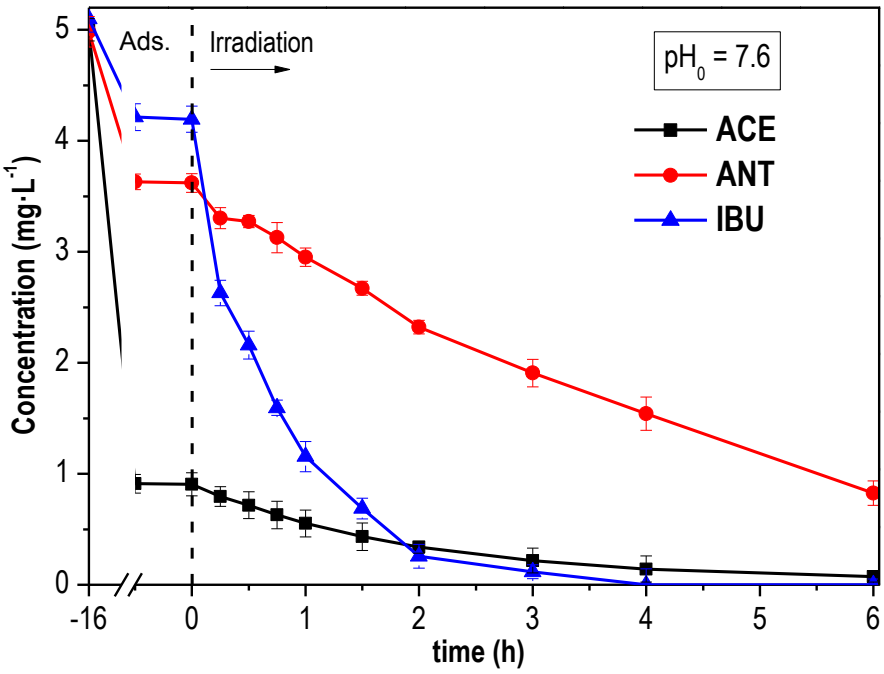

Figure 8. Adsorption and solar photocatalytic degradation of ACE, IBU and ANT with TiO_2/AC-MW (250 mg·L^{-1} of TiO_2) from an aqueous solution of the three compounds (Intensity of irradiation: 600 W·m^{-2}).

Table 5. Values of the first order rate constant, (h^{-1}), of disappearance and TOC removal after 6 h from the experiments of Figure 8 and 9.

Initial pH	ACE	IBU	ANT	TOC removal (%)
3	0.37	--	1.00	23.3
5	0.39	--	0.81	41.5
7.6	0.49	1.33	0.23	48.8
9	0.72	1.00	0.37	42.3
11	0.88	0.53	0.32	16.9

Similar experiments to those of Figure 8 were repeated at different initial pH values. The results are depicted in Figure 9. As can be seen, this variable affected significantly to both adsorption and photocatalytic degradation. At the starting concentration used, IBU was almost completely removed from solution by adsorption at pH ≤ 5. At alkaline pH adsorption decreases because of the electrostatic repulsion between the anionic IBU species (pK_a=4.4) and the catalyst surface (pH_{pzc}=7.0, Figure S5 of Supplementary

Information). Of course, adsorption is not only determined by electrostactic forces but dispersive interactions can be also important depending on the structure of the adsorbate and taking into account, among other, donor-acceptor mechanisms involving π electrons of the aromatic ring of the target compounds (in this case) as well as of the graphene-like layers of activated carbon. That complex force-balance could explain some discontinuities observed in the evolution of adsorption vs pH, moreover, taking also into account the occurrence of competitive adsorption. The size and conformation of the target compound can also influence the adsorption capacity considering the essentially microporous texture of the AC component of the heterostructure. Information on the chemical structure and 3D conformation of the three pharmaceuticals has been included in Supplementary Information (Figure S1). ACE is a p-aminophenol derivative with a planar configuration [55], IBU is a propionic acid derivative with a flexible configuration due to the presence of several torsional twists [56] and ANT is a pyrazolone derivative with a coplanar configuration [57]. Apparently, the flexibility of the IBU favors its adsorption on the surface of the catalyst. Regarding the photocatalytic performance of TiO_2/AC-MW for the degradation of pharmaceuticals mixture at different initial pH, Table 5 collects the values of the first order kinetic constant describing the rate of disappearance of each pharmaceutical and the overall TOC removal after 6 h of solar irradiation. As can be seen ANT undergoes faster and complete conversion at low initial pH values while ACE degradation is favored at high pH. IBU shows the highest degradation rate at medium pH, but its almost complete adsorption at low pH impeded learning on its photocatalytic degradation at these low pH values.

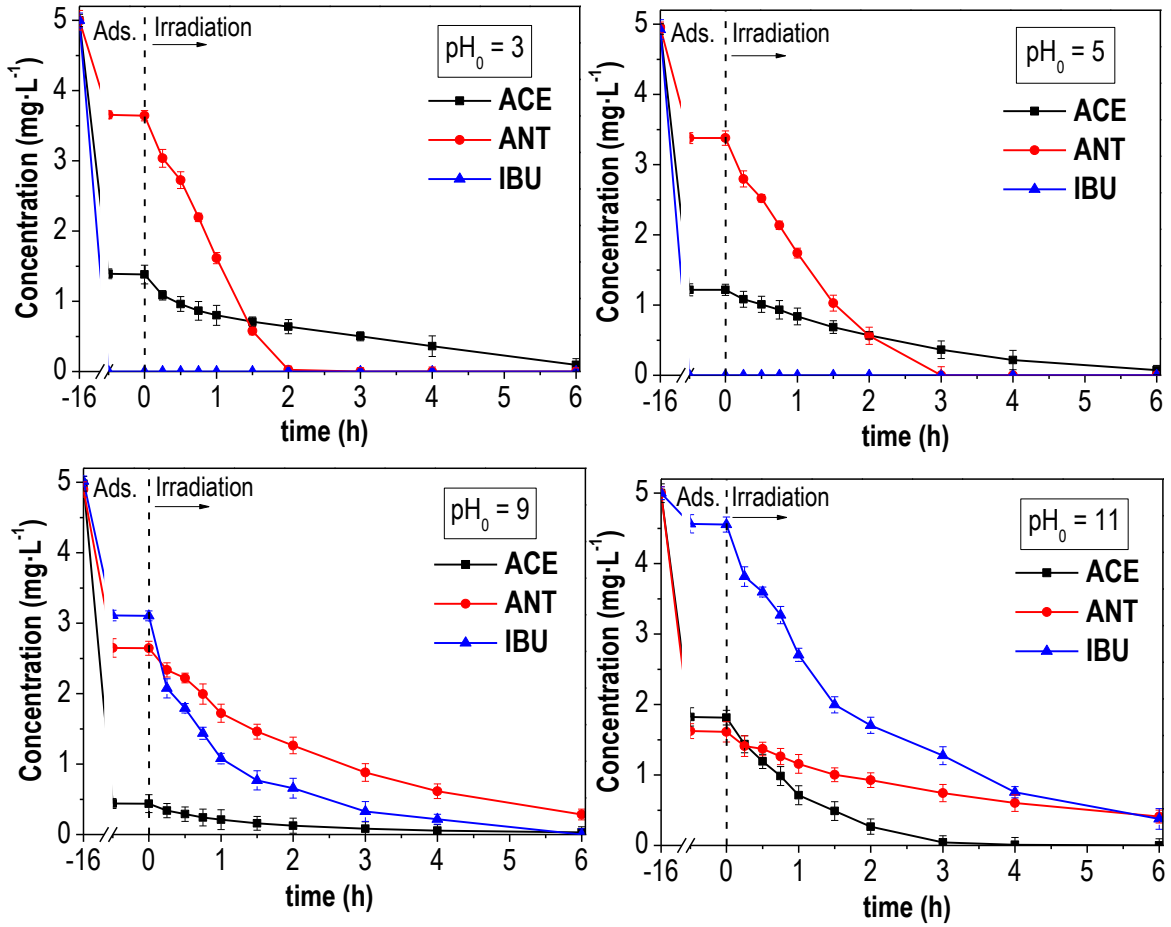

Figure 9. Adsorption and solar photocatalytic degradation of ACE, IBU and ANT with TiO_2/AC-MW at different initial pH values from aqueous solution of the three compounds.

3.3. Photocatalytic intermediates and degradation pathway

The intermediate products in the photocatalytic degradation pathways of the three pharmaceuticals (individual experiments at initial concentration of 100 $mg \cdot L^{-1}$ and pH ≈7) using TiO_2/AC-MW were identified by LC/ESI-MS and IC. The accurate mass of the intermediates are listed, with the corresponding proposed compounds, in Tables S2-4 of the Supplementary Information. The assessment of the chemical species can be considered highly confident taking into account the low mass error (mainly < ±1 mDa) and the value of ring and double bond (RDB). This last parameter corresponds to the number of rings and double bonds existing in a molecule (e.g., parent ACE has a RDB of 5, attributed to the aromatic ring (3 correspond to the double bonds and 1 to the ring) and the double bond C=O in the acetamide group).

For ACE photodegradation, the peaks detected and their proposed identification are collected in Table S2 and the feasible degradation pathways are shown in Figure 10. The ring opening of ACE results in the formation of ACE-1 (protonated form with m/z 118.0857, see Table S2) and succinic and malonic acids. The presence of these acids was also observed in previous studies [59,61,62]. Further oxidation and mineralization of these intermediates lead the formation of acetic and formic acids, and finally CO_2, NO_3^- and H_2O. In addition, the evolution of the short-chain carboxylic acids and NO_3^- has been included in the Supplementary Information (Figure S6a). It can be observed the rapid appearance of succinic acid in the first 15 min of photocatalytic treatment, which disappears along the reaction time, giving rise to the formation of other short-chain acids. It is important to remark that nitrite (NO_2^-) was never detected, being only nitrate (NO_3^-) the resulting mineralized product from the N-C moiety of the initial ACE. Other intermediates identified are derived from the coupling of ACE. Two isomers of ACE-2 (m/z 301.1179) coupling product have been detected, as previously reported by Chen et al. [63], whose photodegradation derived on other products following up to three different pathways: i) the loss of one of the acetamide groups followed by hydroxylation, leading to the formation of ACE-3 (m/z 260.0914); ii) direct aromatic ring hydroxylation, giving rise to the detected intermediates ACE-4 and ACE-5 (m/z 317.1130 and 349.1029, respectively); and iii) further coupling reaction leading to ACE-6 (m/z 450.1653), being identified 3 isomers. The resistance to photocatalytic oxidation of these coupled products can explain the slight reduction of TOC observed in the long-term photocatalytic process (Figure S4). Unlike other reported works dealing with ACE degradation, no products derived from the direct hydroxylation of the ACE aromatic ring were identified (e.g., hydroquinone) [58–61].

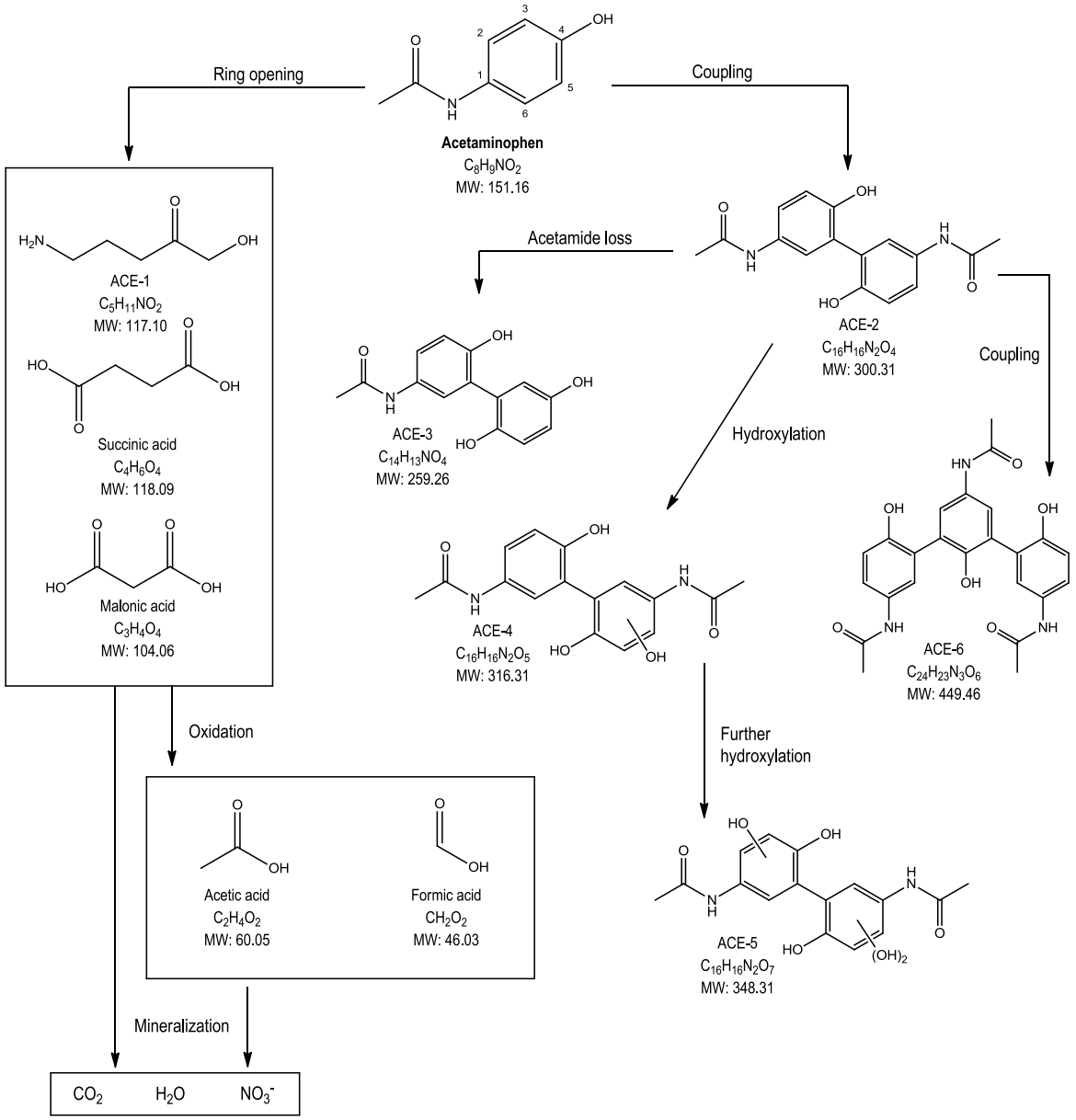

Figure 10. Proposed pathways for solar photocatalytic degradation of ACE with TiO_2/AC-MW.

In contrast to ACE, no coupled intermediates were observed in the degradation pathways of IBU (Figure 11 and Table S3). The hydroxylation of the parent IBU has been the most common oxidative process reported in literature [64–67]. A first degradation pathway can be illustrated through the hydroxylation of ^{7}C in the original structure, resulting in the formation of monohydroxylated ibuprofen [66], identified as IBU-1 (m/z 221.1191, highlights that the ionization for IBU was in negative mode). According to the previous work of Tanveer et al. [67] and Lei et al. [68], the decarboxylation of ^{11}C in IBU-1 is expected to result in the formation of IBU-1* (1-(4-ethyl-phenyl)-2-methyl-propan-1-ol;

m/z 177.1285), which was not detected in our work. However, the product from demethylation of ^{8}C in IBU-1* was identified as IBU-2 (m/z 161.0980), as well as two isomers of IBU-3 (m/z 133.0666), after dealkylation of ^{7}C in IBU-2. A previous toxicity assessment was performed by Da Silva et al.[69], showing that these ibuprofen photocatalytic degradation intermediates had lower ecotoxicity in *Artemia salina* than the parent pharmaceutical. Finally, the IC results showed that the ring cleavage of these compounds leads to the formation of the short-chain carboxylic acids, namely succinic, malonic, acetic and formic. As can be observed in Figure S6b, the concentration of formic acid in the case of IBU degradation was the highest detected from the three pharmaceuticals after 6 h under simulated solar light, consistent with the higher removal of this compound compared to the other two contaminants tested. Further oxidation leads to, CO_2 and H_2O. Ibuprofen can be also degraded by the opening of the phenyl ring, giving IBU-4 (m/z 237.1142). It has to be remarked that this reaction intermediate has not been previously identified in the literature. In addition, the oxidation of the –CHO groups in this intermediate after the ring cleavage results in IBU-5 (m/z 269.1043), which can be further oxidized up to short-chain carboxylic acids, as previously indicated. According to the results of the LC/ESI-MS spectrometry, a third degradation route can be proposed for the original ibuprofen, consisting in a first demethylation of the ^{8}C, giving IBU-6 (m/z 191.1086). Then, a second dealkylation step of the ^{3}C leads to the formation of IBU-7 (m/z 149.0616), which upon further ring opening can also yield ~~to~~ short-chain carboxylic acids, further mineralized.

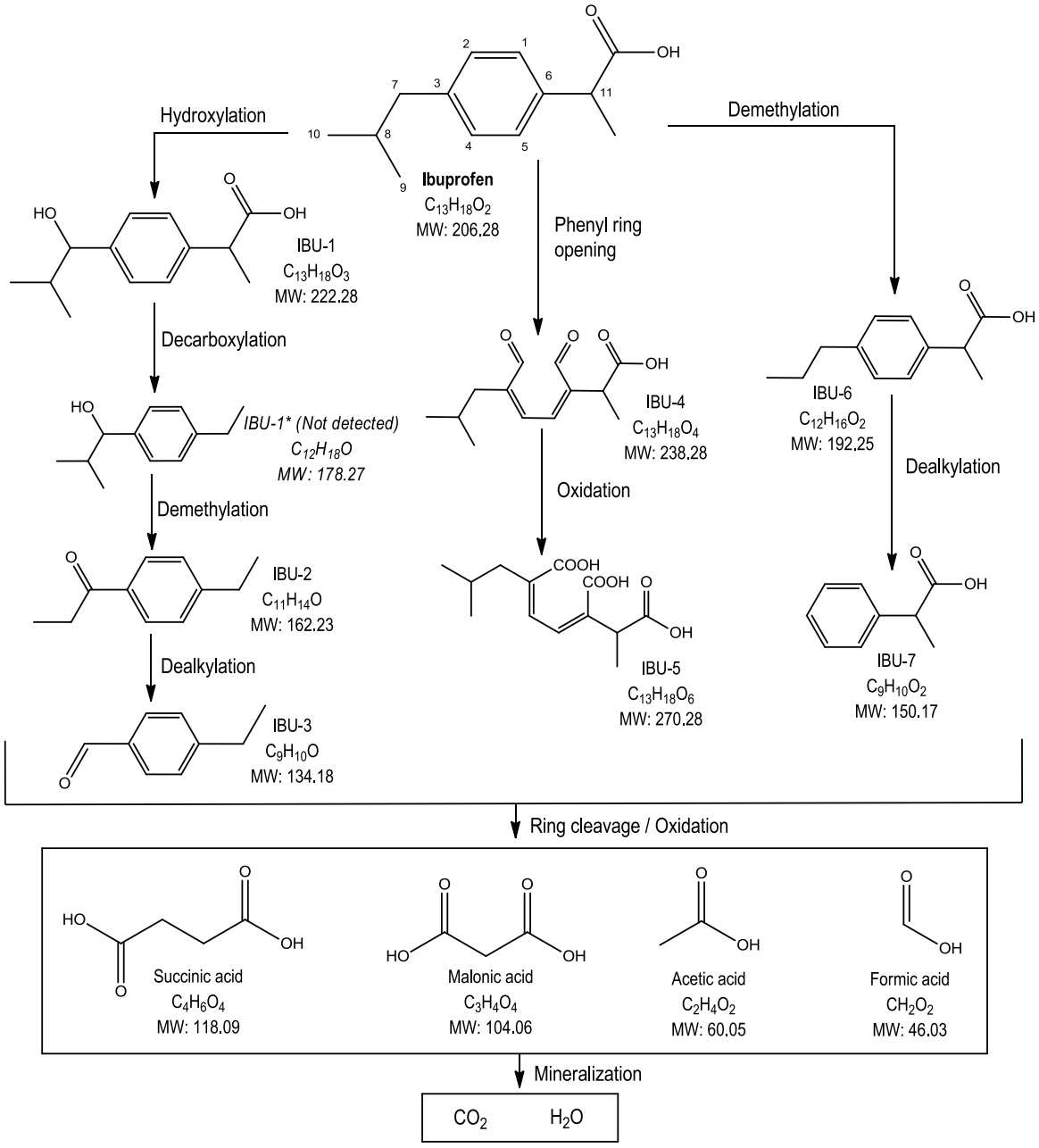

Figure 11. Proposed degradation pathways for solar photocatalytic degradation of IBU with TiO_2/AC-MW.

The proposed photocatalytic degradation pathways of the third pharmaceutical tested in this work, ANT, are shown in Figure 12 (and the identified intermediates listed in Table S4). Three degradation routes are proposed also in this case. In the first one, the loss of the phenyl ring gives rise to the formation of ANT-1 (m/z 113.0689). This compound results from the break of the ^{1}N-^{6}C bond and can be further oxidized to succinic, acetic and formic acids and subsequently to final mineralization products (CO_2, H_2O and NO_3^-) after opening of the pyrazole ring. The evolution of the short-chain carboxylic acids can be

followed in Figure S6c, where it can be seen a different route for the removal of succinic acid compared to that in the case of ACE and IBU. The lower degradation of succinic acid can be one of the possible reasons of the lower TOC removal observed for ANT compared to the other two pharmaceuticals (as previously seen in Figures 5 and 7). On the other hand, and as in the case of ACE, no nitrite was detected in the IC chromatograms. In the second degradation pathway proposed, the cleavage of the pyrazole ring leads to the formation of ANT-2 (m/z 221.0917), which can be degraded by two different ways. On the one hand, through the loss of the oxamoyl chain, giving ANT-3 (m/z 165.1018), as previously reported by Miao et al. [70]. In our current study, a further degradation compound, after double methylation, was observed, listed as ANT-4 (m/z 137.0706). On the other hand, through hydroxylation of the –CHO group in ANT-2, leading to the formation of ANT-5 (m/z 237.0867). In addition, this intermediate can yield the previously indicated ANT-3, after the loss of the 2-oxoacetic acid group in ^{1}N. The third route for the degradation of the parent antipyrine consists of its mono-hydroxylation [70,71]. In the degradation pathway described in the current work, if the hydroxylation of parent ANT occurs in the ^{4}C, ANT-6 (m/z 205.0967) could be formed, which can result in ANT-5 by the cleavage of the pyrazole ring. Moreover, that can also allow the formation of ANT-7 (m/z 393.1559), by coupling of two ANT-6 molecules. In contrast, if the hydroxylation takes place in the aromatic ring of the original ANT, that can lead to 3 isomer structures (ANT 8, m/z 205.0963). Further hydroxylation on ANT-8 would result in the formation of ANT-9 (m/z 221.0917). The oxidation of the listed intermediates leads to the formation of short-chain acids and mineralized products, as previously commented. It has to be remarked that, unlike other degradation pathways of antipyrine found in literature [72–74], anthranilic or 1,4-benzenedicarboxylic acids were not detected.

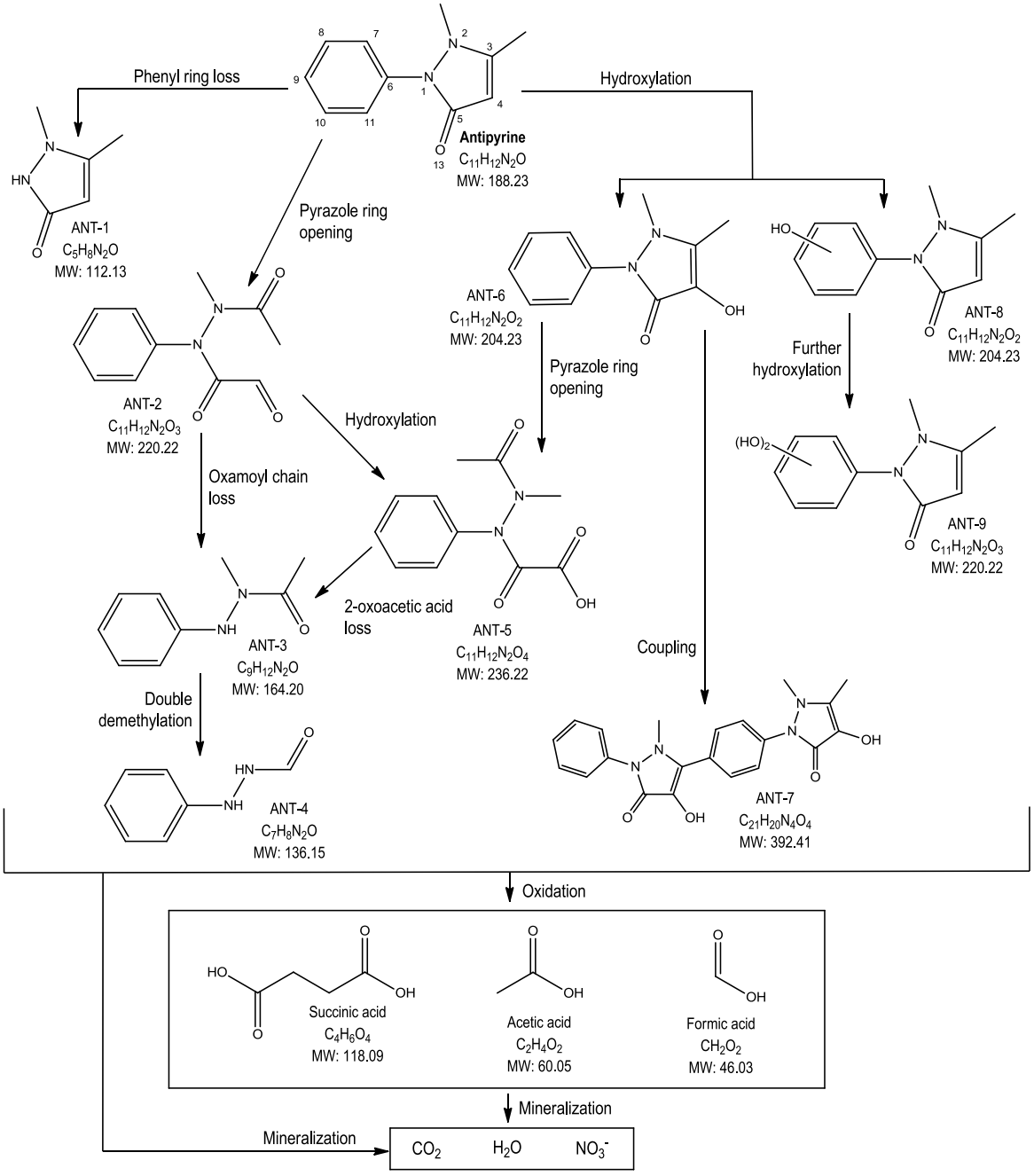

Figure 12. Proposed pathways for solar photocatalytic degradation of ANT with TiO_2/AC-MW.

4. Conclusions

Heterostructures based on TiO_2 supported on activated carbon (TiO_2/AC) have been successfully synthesized through three different procedures (solvothermal, microwave-assisted and sol-gel), using lignin as carbonaceous precursor. All the heterostructures contained anatase as the only crystalline phase. TiO_2/AC-ST and TiO_2/AC-MW samples

have similar properties, characterized by a predominantly mesoporous texture but with significant contribution of microporosity basically associated to the AC component. They are characterized by low TiO_2 crystal size (10 nm) and mean particle size close to 0.25 μm, with a band gap ranging within 3.28-3.38 eV, close to that of bare TiO_2. The heterostructure synthesized by a sol-gel route showed some slight differences, such as higher crystal and particle sizes and lower surface area, most probably due to the higher temperature reached during the heat-treatment included in this synthesis route to achieve anatase crystallization. Regarding the photocatalytic activity, the heterostructure synthesized by a microwave-assisted route (TiO_2/AC-MW) yielded the best performance in the solar-driven photocatalytic degradation of the three pharmaceuticals tested (ACE, IBU and ANT), both in terms of parent compound disappearance (conversion) and mineralization. The best results were obtained for IBU degradation, with complete conversion in less than 3 h, while ANT was found the most recalcitrant.

The degradation pathways proposed for ACE suggest a rapid ring opening leading to the mineralization products (CO_2, H_2O and NO_3^-). However, this mineralization is affected by the generation of coupled intermediates. In the case of IBU, its degradation takes place ~~is~~ mainly through hydroxylation and dealkylation reactions, giving rise to easier ring cleavage to form short-chain carboxylic acids and further mineralization products. Meanwhile, the degradation route for ANT involves a fast opening of the pyrazole ring instead of the phenyl one, in parallel to hydroxylation of the original structure of ANT and the formation of coupled byproducts with apparent high resistance to photocatalytic oxidation.

The performance of TiO_2/AC-MW was also evaluated with a mixture of the three pharmaceuticals at different initial pH values. The highest disappearance rate and overall TOC removal occurred at pH between 7 and 9. Microwave-assisted synthesis can be considered a fast and simple route for preparing heterostructures with promising photocatalytic activity for the abatement of these CECs under solar light.

Supplementary Information

Table S1. Kinetic modelling results of the pseudo-first and second order adsorption of the three contaminants on TiO_2/AC-MW heterostructure.

Table S2. Accurate mass (m/z) values obtained for ACE and its proposed photocatalytic degradation products with the TiO_2/AC-MW heterostructure.

Table S3. Accurate mass (m/z) values obtained for IBU and its proposed photocatalytic degradation products with the TiO_2/AC-MW heterostructure.

Table S4. Accurate mass (m/z) values obtained for ANT and its proposed photocatalytic degradation products with the TiO_2/AC-MW heterostructure.

Figure S1. Chemical structure and 3D conformation of acetaminophen, ibuprofen and antipyrine, from PubChem open chemistry database, National Institutes of Health (NIH).

Figure S2. Low-magnification SEM images of (a) TiO_2/AC-ST, (b) TiO_2/AC-MW and (c) TiO_2/AC-SG.

Figure S3. Experimental adsorption data of the different contaminants on TiO_2/AC-MW heterostructure.

Figure S4. Conversion values for TOC, ACE, IBU and ANT with TiO_2/AC-MW at pH 7.6 from aqueous solution of the three compounds at different irradiation times.

Figure S5. Determination of pH_{pzc} for TiO_2/AC-ST and TiO_2/AC-MW.

Figure S6. Evolution of short-chain organic acids and nitrate (NO_3^-) concentration upon solar photocatalytic degradation with TiO_2/AC-MW of: a) ACE, b) IBU, c) ANT. (Initial concentration of each pharmaceutical = 100 $mg \cdot L^{-1}$).

Acknowledgements

The authors acknowledge the financial support from Spanish MINECO (project CTQ2016-78576-R). M. Peñas-Garzón thanks Spanish MECD for FPU16/00576 grant. Authors thank the Research Support Services of the University of Extremadura (SAIUEx) for its technical and scientific support.

References

[1] Y. Yang, Y.S. Ok, K.H. Kim, E.E. Kwon, Y.F. Tsang, Occurrences and removal of pharmaceuticals and personal care products (PPCPs) in drinking water and water/sewage treatment plants: A review, Sci. Total Environ. 596–597 (2017) 303–320. doi:10.1016/j.scitotenv.2017.04.102.

[2] S.D. Richardson, T.A. Ternes, Water Analysis: Emerging Contaminants and Current Issues, Anal. Chem. 90 (2018) 398–428. doi:10.1021/acs.analchem.7b04577.

[3] S. Mompelat, B. Le Bot, O. Thomas, Occurrence and fate of pharmaceutical products and by-products, from resource to drinking water, Environ. Int. 35 (2009) 803–814. doi:10.1016/j.envint.2008.10.008.

[4] M. Papageorgiou, C. Kosma, D. Lambropoulou, Seasonal occurrence, removal, mass loading and environmental risk assessment of 55 pharmaceuticals and personal care products in a municipal wastewater treatment plant in Central Greece, Sci. Total Environ. 543 (2016) 547–569. doi:10.1016/j.scitotenv.2015.11.047.

[5] N.A. Alygizakis, P. Gago-Ferrero, V.L. Borova, A. Pavlidou, I. Hatzianestis, N.S. Thomaidis, Occurrence and spatial distribution of 158 pharmaceuticals, drugs of abuse and related metabolites in offshore seawater, Sci. Total Environ. 541 (2016) 1097–1105. doi:10.1016/j.scitotenv.2015.09.145.

[6] J.C.G. Sousa, A.R. Ribeiro, M.O. Barbosa, M.F.R. Pereira, A.M.T. Silva, A review on environmental monitoring of water organic pollutants identified by EU guidelines, J. Hazard. Mater. 344 (2018) 146–162. doi:10.1016/j.jhazmat.2017.09.058.

[7] S. Sifakis, V.P. Androutsopoulos, A.M. Tsatsakis, D.A. Spandidos, Human exposure to endocrine disrupting chemicals: effects on the male and female reproductive systems, Environ. Toxicol. Pharmacol. 51 (2017) 56–70. doi:10.1016/j.etap.2017.02.024.

[8] A. Durán, J.M. Monteagudo, I. San Martín, Operation costs of the solar photo-catalytic degradation of pharmaceuticals in water: A mini-review, Chemosphere. 211 (2018) 482–488. doi:10.1016/j.chemosphere.2018.07.170.

[9] T. Deblonde, C. Cossu-Leguille, P. Hartemann, Emerging pollutants in wastewater: A review of the literature, Int. J. Hyg. Environ. Health. 214 (2011) 442–448. doi:10.1016/j.ijheh.2011.08.002.

[10] U.N.G. Assembly, Transforming our world: the 2030 Agenda for Sustainable Development, 2015. https://www.unfpa.org/sites/default/files/resource-pdf/Resolution_A_RES_70_1_EN.pdf (accessed April 10, 2019).

[11] L. Rizzo, S. Malato, D. Antakyali, V.G. Beretsou, M.B. Đolić, W. Gernjak, E. Heath, I. Ivancev-Tumbas, P. Karaolia, A.R. Lado Ribeiro, G. Mascolo, C.S. McArdell, H. Schaar, A.M.T. Silva, D. Fatta-Kassinos, Consolidated vs new advanced treatment methods for the removal of contaminants of emerging concern from urban wastewater, Sci. Total Environ. 655 (2019) 986–1008. doi:10.1016/j.scitotenv.2018.11.265.

[12] Z. Cai, A.D. Dwivedi, W.-N. Lee, X. Zhao, W. Liu, M. Sillanpää, D. Zhao, C.-H. Huang, J. Fu, Application of nanotechnologies for removing pharmaceutically active compounds from water: development and future trends, Environ. Sci. Nano. 5 (2018) 27–47. doi:10.1039/C7EN00644F.

[13] C. Byrne, G. Subramanian, S.C. Pillai, Recent advances in photocatalysis for environmental applications, J. Environ. Chem. Eng. 6 (2018) 3531–3555. doi:10.1016/j.jece.2017.07.080.

[14] H. Dong, G. Zeng, L. Tang, C. Fan, C. Zhang, X. He, Y. He, An overview on limitations of TiO2-based particles for photocatalytic degradation of organic pollutants and the corresponding countermeasures, Water Res. 79 (2015) 128–146. doi:10.1016/j.watres.2015.04.038.

[15] B. Srikanth, R. Goutham, R. Badri Narayan, A. Ramprasath, K.P. Gopinath, A.R. Sankaranarayanan, Recent advancements in supporting materials for immobilised photocatalytic applications in waste water treatment, J. Environ. Manage. 200 (2017) 60–78. doi:10.1016/j.jenvman.2017.05.063.

[16] C. Belver, J. Bedia, J.J. Rodriguez, Titania-clay heterostructures with solar photocatalytic applications, Appl. Catal. B Environ. 176–177 (2015) 278–287. doi:10.1016/j.apcatb.2015.04.004.

[17] F.J. García-Mateos, R. Berenguer, M.J. Valero-Romero, J. Rodríguez-Mirasol, T. Cordero, Phosphorus functionalization for the rapid preparation of highly nanoporous submicron-diameter carbon fibers by electrospinning of lignin solutions, J. Mater. Chem. A. 6 (2018) 1219–1233. doi:10.1039/c7ta08788h.

[18] F. García-Mateos, I. Moulefera, J. Rosas, A. Benyoucef, J. Rodríguez-Mirasol, T. Cordero, Alcohol Dehydrogenation on Kraft Lignin-Derived Chars with Surface Basicity, Catalysts. 7 (2017) 308. doi:10.3390/catal7100308.

[19] D.A. Baker, T.G. Rials, Recent advances in low-cost carbon fiber manufacture from lignin, J. Appl. Polym. Sci. 130 (2013) 713–728. doi:10.1002/app.39273.

[20] J.M. Rosas, R. Berenguer, M.J. Valero-Romero, J. Rodríguez-Mirasol, T. Cordero, Preparation of Different Carbon Materials by Thermochemical Conversion of Lignin, Front. Mater. 1 (2014) 1–17. doi:10.3389/fmats.2014.00029.

[21] R. Ruiz-Rosas, J. Bedia, M. Lallave, I.G. Loscertales, A. Barrero, J. Rodríguez-Mirasol, T. Cordero, The production of submicron diameter carbon fibers by the electrospinning of lignin, Carbon N. Y. 48 (2010) 696–705. doi:10.1016/j.carbon.2009.10.014.

[22] F.J. García-Mateos, T. Cordero-Lanzac, R. Berenguer, E. Morallón, D. Cazorla-Amorós, J. Rodríguez-Mirasol, T. Cordero, Lignin-derived Pt supported carbon (submicron)fiber electrocatalysts for alcohol electro-oxidation, Appl. Catal. B Environ. 211 (2017) 18–30. doi:10.1016/j.apcatb.2017.04.008.

[23] C. Fernandez-Ruiz, J. Bedia, P. Bonal, J.J. Rodriguez, L.M. Gómez-Sainero, Chloroform conversion into ethane and propane by catalytic hydrodechlorination with Pd supported on activated carbons from lignin, Catal. Sci. Technol. 8 (2018) 3926–3935. doi:10.1039/C8CY00461G.

[24] J.M. Rosas, R. Ruiz-Rosas, J. Rodríguez-Mirasol, T. Cordero, Kinetic study of SO_2 removal over lignin-based activated carbon, Chem. Eng. J. 307 (2017) 707–721. doi:10.1016/j.cej.2016.08.111.

[25] J.J. Rodríguez, T. Cordero, J. Rodríguez-Mirasol, Carbon Materials from Lignin and Their Applications, Biofuels and Biorefineries. 6 (2016). doi:10.1007/978-981-10-1965-4_8.

[26] Suhas, P.J.M. Carrott, M.M.L. Ribeiro Carrott, Lignin - from natural adsorbent to activated carbon: A review, Bioresour. Technol. 98 (2007) 2301–2312. doi:10.1016/j.biortech.2006.08.008.

[27] M. Peñas-Garzón, A. Gómez-Avilés, J.B. Garcia-Matamoros, J.J. Rodriguez, C. Belver, Effect of Activating Agent on the Properties of TiO_2/Activated Carbon Heterostructures for Solar Photocatalytic Degradation of Acetaminophen, Materials (Basel). (2019). doi:10.3390/ma12030378.

[28] D. Awfa, M. Ateia, M. Fujii, M.S. Johnson, C. Yoshimura, Photodegradation of pharmaceuticals and personal care products in water treatment using carbonaceous-TiO2 composites: A critical review of recent literature, Water Res. 142 (2018) 26–45. doi:10.1016/j.watres.2018.05.036.

[29] A. Rey, D.H. Quiñones, P.M. Álvarez, F.J. Beltrán, P.K. Plucinski, Simulated solar-light assisted photocatalytic ozonation of metoprolol over titania-coated magnetic activated carbon, Appl. Catal. B Environ. 111–112 (2012) 246–253. doi:10.1016/j.apcatb.2011.10.005.

[30] S.X. Liu, X.Y. Chen, X. Chen, A TiO2/AC composite photocatalyst with high activity and easy separation prepared by a hydrothermal method, J. Hazard. Mater. 143 (2007) 257–263. doi:10.1016/j.jhazmat.2006.09.026.

[31] A. Omri, S.D. Lambert, J. Geens, F. Bennour, M. Benzina, Synthesis, surface characterization and Photocatalytic activity of TiO2 supported on Almond shell

activated carbon, J. Mater. Sci. Technol. 30 (2014) 894–902. doi:10.1016/j.jmst.2014.04.007.

[32] C. Orha, R. Pode, F. Manea, C. Lazau, C. Bandas, Titanium dioxide-modified activated carbon for advanced drinking water treatment, Process Saf. Environ. Prot. 108 (2017) 26–33. doi:10.1016/j.psep.2016.07.013.

[33] J. Bedia, C. Belver, S. Ponce, J. Rodriguez, J.J. Rodriguez, Adsorption of antipyrine by activated carbons from FeCl3-activation of Tara gum, Chem. Eng. J. 333 (2018) 58–65. doi:10.1016/j.cej.2017.09.161.

[34] J. Bedia, V.M. Monsalvo, J.J. Rodriguez, A.F. Mohedano, Iron catalysts by chemical activation of sewage sludge with FeCl3for CWPO, Chem. Eng. J. 318 (2017) 224–230. doi:10.1016/j.cej.2016.06.096.

[35] J.A. Zazo, J. Bedia, C.M. Fierro, G. Pliego, J.A. Casas, J.J. Rodriguez, Highly stable Fe on activated carbon catalysts for CWPO upon FeCl3 activation of lignin from black liquors, Catal. Today. 187 (2012) 115–121. doi:10.1016/j.cattod.2011.10.003.

[36] S. Brunauer, P.H. Emmett, E. Teller, Adsorption of Gases in Multimolecular Layers, J. Am. Chem. Soc. 60 (1938) 309–319. doi:10.1021/ja01269a023.

[37] B.C. Lippens, de B. J.H., Studies on pore systems in catalysts: V. The t method, J. Catal. 4 (1965) 319–323. doi:10.1016/0021-9517(65)90307-6.

[38] J. Tauc, Absorption edge and internal electric fields in amorphous semiconductors, Mater. Res. Bull. 5 (1970) 721–729. doi:10.1016/0025-5408(70)90112-1.

[39] J. Zhang, P. Zhou, J. Liu, J. Yu, New understanding of the difference of photocatalytic activity among anatase, rutile and brookite TiO2, Phys. Chem. Chem. Phys. 16 (2014) 20382–20386. doi:10.1039/c4cp02201g.

[40] G. Newcombe, R. Hayes, M. Drikas, Granular activated carbon: Importance of surface properties in the adsorption of naturally occurring organics, Colloids Surfaces A Physicochem. Eng. Asp. 78 (1993) 65–71. doi:10.1016/0927-7757(93)80311-2.

[41] F. Tian, Z. Wu, Q. Chen, Y. Yan, G. Cravotto, Z. Wu, Microwave-induced crystallization of AC/TiO_2 for improving the performance of rhodamine B dye degradation, Appl. Surf. Sci. 351 (2015) 104–112. doi:10.1016/j.apsusc.2015.05.133.

[42] D. Liu, Z. Wu, F. Tian, B.C. Ye, Y. Tong, Synthesis of N and La co-doped TiO_2/AC photocatalyst by microwave irradiation for the photocatalytic degradation

of naphthalene, J. Alloys Compd. 676 (2016) 489–498. doi:10.1016/j.jallcom.2016.03.124.

[43] S. Horikoshi, S. Sakamoto, N. Serpone, Formation and efficacy of TiO2/AC composites prepared under microwave irradiation in the photoinduced transformation of the 2-propanol VOC pollutant in air, Appl. Catal. B Environ. 140–141 (2013) 646–651. doi:10.1016/j.apcatb.2013.04.060.

[44] M. Thommes, K. Kaneko, A. V. Neimark, J.P. Olivier, F. Rodriguez-Reinoso, J. Rouquerol, K.S.W. Sing, Physisorption of gases, with special reference to the evaluation of surface area and pore size distribution (IUPAC Technical Report), Pure Appl. Chem. 87 (2015) 1051–1069. doi:10.1515/pac-2014-1117.

[45] A.C. Martins, A.L. Cazetta, O. Pezoti, J.R.B. Souza, T. Zhang, E.J. Pilau, T. Asefa, V.C. Almeida, Sol-gel synthesis of new TiO2/activated carbon photocatalyst and its application for degradation of tetracycline, Ceram. Int. 43 (2017) 4411–4418. doi:10.1016/j.ceramint.2016.12.088.

[46] R. Leary, A. Westwood, Carbonaceous nanomaterials for the enhancement of TiO_2 photocatalysis, Carbon N. Y. 49 (2011) 741–772. doi:10.1016/j.carbon.2010.10.010.

[47] N.R. Khalid, A. Majid, M.B. Tahir, N.A. Niaz, S. Khalid, Carbonaceous-TiO_2 nanomaterials for photocatalytic degradation of pollutants: A review, Ceram. Int. 43 (2017) 14552–14571. doi:10.1016/j.ceramint.2017.08.143.

[48] M. Akkari, P. Aranda, C. Belver, J. Bedia, A. Ben Haj Amara, E. Ruiz-Hitzky, ZnO/sepiolite heterostructured materials for solar photocatalytic degradation of pharmaceuticals in wastewater, Appl. Clay Sci. 156 (2018) 104–109. doi:10.1016/j.clay.2018.01.021.

[49] C. Belver, J. Bedia, J.J. Rodriguez, Zr-doped TiO2 supported on delaminated clay materials for solar photocatalytic treatment of emerging pollutants, J. Hazard. Mater. 322 (2017) 233–242. doi:10.1016/j.jhazmat.2016.02.028.

[50] A. Gómez-Avilés, M. Peñas-Garzón, J. Bedia, D.D. Dionysiou, J.J. Rodríguez, C. Belver, Mixed Ti-Zr metal-organic-frameworks for the photodegradation of acetaminophen under solar irradiation, Appl. Catal. B Environ. 253 (2019) 253–262. doi:10.1016/j.apcatb.2019.04.040.

[51] N. Jallouli, K. Elghniji, H. Trabelsi, M. Ksibi, Photocatalytic degradation of paracetamol on TiO2 nanoparticles and TiO2/cellulosic fiber under UV and sunlight irradiation, Arab. J. Chem. 10 (2017) S3640–S3645.

doi:10.1016/j.arabjc.2014.03.014.
[52] C. Belver, M. Hinojosa, J. Bedia, M. Tobajas, M.A. Alvarez, V. Rodríguez-González, J.J. Rodriguez, Ag-Coated heterostructures of ZnO-TiO2/delaminated montmorillonite as solar photocatalysts, Materials (Basel). 10 (2017) 960. doi:10.3390/ma10080960.
[53] A. Eslami, M.M. Amini, A.R. Yazdanbakhsh, A. Mohseni-Bandpei, A.A. Safari, A. Asadi, N,S co-doped TiO2 nanoparticles and nanosheets in simulated solar light for photocatalytic degradation of non-steroidal anti-inflammatory drugs in water: a comparative study, J. Chem. Technol. Biotechnol. 91 (2016) 2693–2704. doi:10.1002/jctb.4877.
[54] G. Di, Z. Zhu, H. Zhang, J. Zhu, H. Lu, W. Zhang, Y. Qiu, L. Zhu, S. Küppers, Simultaneous removal of several pharmaceuticals and arsenic on Zn-Fe mixed metal oxides: Combination of photocatalysis and adsorption, Chem. Eng. J. 328 (2017) 141–151. doi:10.1016/j.cej.2017.06.112.
[55] A.M. Amado, C. Azevedo, P.J.A. Ribeiro-Claro, Conformational and vibrational reassessment of solid paracetamol, Spectrochim. Acta Part A Mol. Biomol. Spectrosc. 183 (2017) 431–438. doi:10.1016/j.saa.2017.04.076.
[56] D.J. Goossens, A.P. Heerdegen, T.R. Welberry, A.G. Beasley, The molecular conformation of Ibuprofen, C13H18O2, through X-ray diffuse scattering, Int. J. Pharm. 343 (2007) 59–68. doi:10.1016/J.IJPHARM.2007.04.023.
[57] K.S. Venkatasubban, R. Rothchild, NMR Studies of Drugs: Antipyrine and Analogs. II. ^{1}H and ^{13}C Chemical Shift Dispersion as Conformation Indicator for the *N* -Phenyl Ring., Spectrosc. Lett. 30 (1997) 1685–1697. doi:10.1080/00387019708006752.
[58] M.M. Hinojosa Guerra, I. Oller Alberola, S. Malato Rodriguez, A. Agüera López, A. Acevedo Merino, A. Egea-Corbacho Lopera, J.M. Quiroga Alonso, Oxidation mechanisms of amoxicillin and paracetamol in the photo-Fenton solar process, Water Res. 156 (2019) 232–240. doi:10.1016/j.watres.2019.02.055.
[59] R. Andreozzi, V. Caprio, R. Marotta, D. Vogna, Paracetamol oxidation from aqueous solutions by means of ozonation and H2O2/UV system, Water Res. 37 (2003) 993–1004. doi:10.1016/S0043-1354(02)00460-8.
[60] S. Wang, J. Wu, X. Lu, W. Xu, Q. Gong, J. Ding, B. Dan, P. Xie, Removal of acetaminophen in the Fe2+/persulfate system: Kinetic model and degradation pathways, Chem. Eng. J. 358 (2019) 1091–1100. doi:10.1016/j.cej.2018.09.145.

[61] H. Lee, I.S. Park, H.J. Bang, Y.K. Park, H. Kim, H.H. Ha, B.J. Kim, S.C. Jung, Fabrication of Gd-La codoped TiO 2 composite via a liquid phase plasma method and its application as visible-light photocatalysts, Appl. Surf. Sci. 471 (2019) 893–899. doi:10.1016/j.apsusc.2018.11.249.

[62] C.T. Chang, J.J. Wang, T. Ouyang, Q. Zhang, Y.H. Jing, Photocatalytic degradation of acetaminophen in aqueous solutions by TiO2/ZSM-5 zeolite with low energy irradiation, Mater. Sci. Eng. B Solid-State Mater. Adv. Technol. 196 (2015) 53–60. doi:10.1016/j.mseb.2014.12.025.

[63] Y. Chen, X. Zhang, L. Mao, Z. Yang, Dependence of kinetics and pathway of acetaminophen photocatalytic degradation on irradiation photon energy and TiO2 crystalline, Chem. Eng. J. 330 (2017) 1091–1099. doi:10.1016/j.cej.2017.07.148.

[64] Y. Xiang, J. Fang, C. Shang, Kinetics and pathways of ibuprofen degradation by the UV/chlorine advanced oxidation process, Water Res. 90 (2016) 301–308. doi:10.1016/j.watres.2015.11.069.

[65] N. Liu, W. Huang, M. Tang, C. Yin, B. Gao, Z. Li, L. Tang, J. Lei, L. Cui, X. Zhang, In-situ fabrication of needle-shaped MIL-53(Fe) with 1T-MoS2 and study on its enhanced photocatalytic mechanism of ibuprofen, Chem. Eng. J. 359 (2019) 254–264. doi:10.1016/j.cej.2018.11.143.

[66] L. Lin, W. Jiang, M. Bechelany, M. Nasr, J. Jarvis, T. Schaub, R.R. Sapkota, P. Miele, H. Wang, P. Xu, Adsorption and photocatalytic oxidation of ibuprofen using nanocomposites of TiO2 nanofibers combined with BN nanosheets: Degradation products and mechanisms, Chemosphere. 220 (2019) 921–929. doi:10.1016/j.chemosphere.2018.12.184.

[67] M. Tanveer, G.T. Guyer, G. Abbas, Photocatalytic degradation of ibuprofen in water using TiO2 and ZnO under artificial UV and solar irradiation, Water Environ. Res. 91 (2019) 822–829. doi:10.1002/wer.1104.

[68] Z. dong Lei, J. jun Wang, L. Wang, X. yu Yang, G. Xu, L. Tang, Efficient photocatalytic degradation of ibuprofen in aqueous solution using novel visible-light responsive graphene quantum dot/AgVO3 nanoribbons, J. Hazard. Mater. 312 (2016) 298–306. doi:10.1016/j.jhazmat.2016.03.044.

[69] J.C.C. Da Silva, J.A.R. Teodoro, R.J. de C.F. Afonso, S.F. Aquino, R. Augusti, Photolysis and photocatalysis of ibuprofen in aqueous medium: Characterization of by-products via liquid chromatography coupled to high-resolution mass spectrometry and assessment of their toxicities against Artemia Salina, J. Mass

Spectrom. 49 (2014) 145–153. doi:10.1002/jms.3320.
[70] H.F. Miao, M. Cao, D.Y. Xu, H.Y. Ren, M.X. Zhao, Z.X. Huang, W.Q. Ruan, Degradation of phenazone in aqueous solution with ozone: Influencing factors and degradation pathways, Chemosphere. 119 (2015) 326–333. doi:10.1016/j.chemosphere.2014.06.082.
[71] H. Gong, W. Chu, M. Chen, Q. Wang, A systematic study on photocatalysis of antipyrine: Catalyst characterization, parameter optimization, reaction mechanism a toxicity evolution to plankton, Water Res. 112 (2017) 167–175. doi:10.1016/j.watres.2017.01.041.
[72] F. Yuan, C. Hu, X. Hu, J. Qu, M. Yang, Degradation of selected pharmaceuticals in aqueous solution with UV and UV/H2O2, Water Res. 43 (2009) 1766–1774. doi:10.1016/j.watres.2009.01.008.
[73] A.J. Expósito, D.A. Patterson, W.S.W. Mansor, J.M. Monteagudo, E. Emanuelsson, I. Sanmartín, A. Durán, Antipyrine removal by TiO2 photocatalysis based on spinning disc reactor technology, J. Environ. Manage. 187 (2017) 504–512. doi:10.1016/j.jenvman.2016.11.012.
[74] J.M. Monteagudo, A. Durán, J. Latorre, A.J. Expósito, Application of activated persulfate for removal of intermediates from antipyrine wastewater degradation refractory towards hydroxyl radical, J. Hazard. Mater. 306 (2016) 77–86. doi:10.1016/j.jhazmat.2015.12.001.

Supplementary Material

Click here to download Supplementary Material: Supplementary- CEJ-D-19-16340.docx

***Declaration of Interest Statement**

Declaration of interests

☒ The authors declare that they have no known competing financial interests or personal relationships that could have appeared to influence the work reported in this paper.

☐The authors declare the following financial interests/personal relationships which may be considered as potential competing interests: